Photocatalytic Degradation and Adsorptive Removal of Emerging Organic Pesticides Using Metal Oxide and Their Composites: Recent Trends and Future Perspectives

Haneen H. Shanaah [1] , **Eman F. H. Alzaimoor** [1] , **Suad Rashdan** [1], **Amina A. Abdalhafith** [2] and **Ayman H. Kamel** [1,3,*]

1   Chemistry Department, College of Science, Sakhir 32038, Bahrain
2   Chemistry Department, Faculty of Arts and Sciences, University of Benghazi, Koufra, Benghazi P.O. Box 1308, Libya
3   Department of Chemistry, Faculty of Science, Ain Shams University, Cairo 11566, Egypt
*   Correspondence: ahkamel76@sci.asu.edu.eg or ahmohamed@uob.edu.bh

Abstract: For applications involving water cleanup, metal oxide nanoparticles are exceptionally successful. They are useful for the adsorption and photocatalytic destruction of organic pollutants due to their distinctive qualities, which include their wide surface/volume area, high number of active sites, porous structure, stability, recovery, and low toxicity. Metal oxide nanomaterials have drawn a lot of attention from researchers in the past ten years because of their various production pathways, simplicity in surface modification, abundance, and inexpensive cost. A wide range of metal oxides, such as iron oxides, MgO, TiO_2, ZnO, WO_3, CuO, Cu_2O, metal oxides composites, and graphene–metal oxides composites, with variable structural, crystalline, and morphological features, are reviewed, emphasizing the recent development, challenges, and opportunities for adsorptive removal and photocatalytic degradation of organic pollutants such as dyes, pesticides, phenolic compounds, and so on. In-depth study of the photocatalytic mechanism of metal oxides, their composites, and photocatalytically important characteristics is also covered in this paper. Metal oxides are particularly effective photocatalysts for the degradation of organic pollutants due to their high photodegradation efficiency, economically sound methods for producing photo-catalytic materials, and precise band-gap engineering. Due to their detrimental effects on human health, pesticides—one of the highly hazardous organic pollutants—play a significant part in environmental contamination. Depending on where they come from and who they are targeting, they are categorized in various ways. Researchers focusing on metal oxides and their composites for the adsorptive and photocatalytic degradation of pesticides would find the review to be a beneficial resource. Detailed information on many pesticides, difficulties associated with pesticides, environmental concentration, and the necessity of degradation has been presented.

Keywords: metal oxide nanomaterials; organic pesticides; photocatalysis; remediation; surface adsorption

1. Introduction

Persistent organic chemicals (POPs) are highly hazardous to the ecosystem and living organisms [1]. Their non-biodegradability allows them to accumulate easily in the food chain, affecting both humans and wildlife [2]. Pesticides are one class of POPs with half-lives that can extend to years [3]. They have been used abundantly to control the growth of the crops by exterminating pests including insects, fungi, and microorganisms in agricultural farms [4]. However, the highly toxic nature of these material has become an alarming concern to humans and the environment since they can readily contaminate soil, air, and water through sewage water and industrial and domestic wastes [5]. Additionally,

pesticides present in water can reach groundwater through leakages and leaching, surface water, and drinkable water [6–8].

The adverse effect of different pesticides on human health have been extensively reported and investigated [9]. For example, organochlorines (OCs) and organophosphates (OPs) accumulate acetylcholine in the central nervous system of humans, leading to serious brain disorder [10]. Carbamates are another class of pesticides that induce apoptosis for human cells and raise the risk of cancer [11]. Other pesticides such as simazine affect humans in trace amounts, leading to kidney failure and heart and lung diseases [12]. Accordingly, numerous attempts have been made to remediate these harmful toxicants from the environmental matrices, utilizing various removal techniques including chemical precipitation, membrane separation, electrocatalysis, advanced oxidation processes, and adsorption [13,14].

The adsorption process has become one of the most researched practices due to its ease of applicability and low cost, depending on the adsorbent [15]. Although adsorption is an easily accessible method for remediation, it generates secondary products and requires further treatment. Accordingly, photocatalytic degradation has attracted the attention of researchers as an alternative technique for the mineralization of toxicants. Photocatalytic degradation employs solar energy, UV, or/and visible light to irradiate a semiconducting material resulting, in the generation of a series of radicals, including hydroxide and superoxide radicals, which are responsible for photodegradation [16]. Studies have shown that photocatalytic activity can be enhanced when the material is adsorbed on the surface of the photocatalyst [17]. Photoactivity, photostability, chemical stability, and the band gap of the photocatalyst should be considered when choosing an adequate material for photocatalytic degradation [18,19]. Photocatalytic degradation can be regarded as a better approach towards the disposing of toxicants; however, it is a more complex process and requires the presence of oxygen as an oxidant [20]. Several studies have corroborated that the higher adsorption capacity of the photocatalyst leads to higher efficiency in degradation, where adsorption facilitates the contact between the pollutant and the photocatalyst. Therefore, a high photodegradation rate requires an effective adsorption process at optimum conditions [21].

Recently, various materials have been investigated for the effective removal of pesticides using adsorption and photocatalytic degradation. Metal oxide nanoparticles, including ferric oxides, cobalt oxides, copper oxides, zinc oxides, titanium oxides, magnesium oxides, cerium oxide, aluminum oxides, and other metal oxides have shown promising removal and degradation results with respect to pollutants such as heavy metals and POPs [22–24]. Likewise, they have been widely implemented as nano-adsorbents and photocatalysts for the remediation of pesticides [17]. Their exquisite physical and chemical properties, influenced by their size (1–100 nm), permit them to differ from their corresponding bulk material [25]. Their eminent properties, including large surface/volume area, high number of active sites, porous structure, stability, recovery, and low toxicity, make them valuable nano-adsorbents and photocatalysts [22,26,27].

Developing the structural properties of nano-adsorbents and photocatalysts has become a demand. Therefore, different strategies have been applied to achieve superior performance in physisorption, in chemisorption, and in reducing the band gaps of the photocatalysts to attain the slow recombination of the charge carriers and enhance photo degradation [28,29]. Doping photocatalysts with different metals [30,31], the multifunctionalization of the surface [32], developing heterostructures [33], developing nanocomposites such as metal oxides/metal-organic frameworks [34], metal oxides/polymers [35], and metal/metal oxides [36], are the main strategies followed to manipulate the characteristics of nano-adsorbents and photocatalysts. Many in vitro and in vivo studies have been conducted recently to better understand the toxicological effects and potential risks of various nanoparticle exposures on people and the environment. There is still a major gap in knowledge about the toxic effects of nanoparticle exposure.

Finding an effective remediation process for the harmful effects of pesticides requires immediate. This review provides a detailed collection of recent references to demonstrate the importance of metal oxides and their functionalized nanocomposites in the removal of different types of pesticides using adsorption and photocatalytic degradation.

2. Nanoarchitectures of Metal Oxides and Oxide Perovskites

2.1. Cobalt Oxide

Cobalt oxides are a type of inorganic metal oxides that exists abundantly in nature. Cobalt oxides have many properties that are favorable to environmental applications; they are highly stable, exert no toxicity, exhibit a magnetic behavior, highly resistant to corrosion and oxidation, and have high mechanical strength [37–39]. They are p-type semiconducting materials at room temperature that show good conductivity [40]. Cobalt oxides have differences in oxygen vacancies; thus, cobalt oxide exists in many oxidation states [41]. Some of the most used oxidation states include cobalt (II) oxide and cobalt (III) oxide [42]. The structure of Co_3O_4 NPs consists of a cubic spinel structure with Co (II) at the tetrahedral sites and Co (III) at the octahedral sites [38,43]. Figure 1 shows the structure of Co_3O_4 spinel structure, with Co (II) surrounded by four oxygen atoms and Co (III), surrounded by six oxygen atoms [44]. Several synthesis methods of cobalt oxide have been reported, including sol–gel, hydrothermal, and microwave-assisted methods. The variable oxidation states of cobalt have made the particles applicable to many fields [45]. Cobalt oxide plays a vital role in many applications, including pollutants sensing, degradation of harmful materials, drug delivery systems, supercapacitors, and storage devices [46–54].
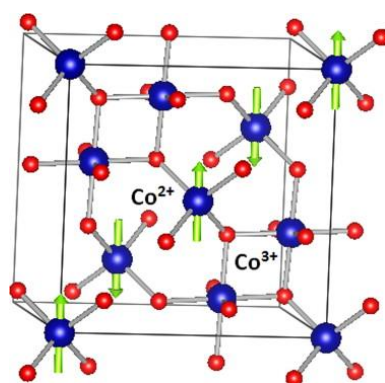
Figure 1. Spinel structure of Co_3O_4 with Co (II) at the tetrahedral sites and Co(III) at the octahedral sites. Reproduced with permission from [44].

2.2. Copper Oxide

Copper oxides exert various properties that make them easily appliable. Numerous structures of copper oxides can be synthesized, such as nanowires, nanorods, nanotubes, and nanoparticles [55]. They are abundant, inexpensive, and highly stable, with high catalytic and antibacterial activity [56]. Different oxidation states of copper oxides are available; however, cuprous oxide (Cu_2O) and cupric oxide (CuO) are the most stable, while paramelaconite (Cu_4O_3) is metastable. Figure 2 shows the three crystal structures for copper oxides [57]. Cuprous oxide (Cu_2O) crystallizes in a cubic structure and is a p-type semiconductor. On the other hand, cupric oxide (CuO) exists in a monoclinic crystal structure and is believed to be both a p- and an n-type semiconductor [58,59]. Figure 3 illustrates the difference between a p-type and an n-type semiconductors.

Copper oxide semiconductors are recognized for their role in the remediation of environmental contaminants due to their strong oxidation and reduction ability and environmental compatibility [60]. A difference between cobalt oxides and copper oxides is that cobalt oxides have higher stability at high temperatures. However, the precursor salts of cobalt oxides are more expensive than the precursor salts of copper oxide, making copper

oxides more easily obtained and applied in many fields [61]. Copper oxides have many prospective applications in the fields of sensors, antimicrobial activity, catalysis, coatings, polymers, and electronics [62–66]. Moreover, cupric oxide shows promising results for the decontamination of water since it is relatively cheap, with high catalytic activity [67,68]. Many routes for the preparation of copper oxides are available. Chemical precipitation, the sonochemical method, hydrothermal synthesis, and synthesis via plant extracts and micro-organisms, are all examples for chemical and biological methods for the synthesis of copper oxide NPs [69,70].
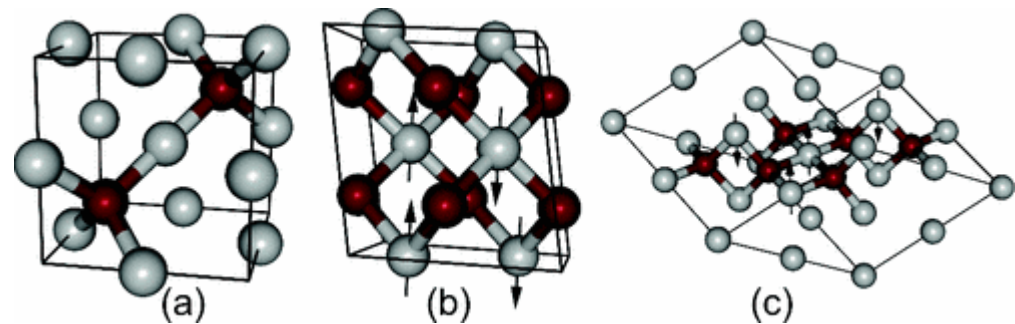
Figure 2. The different structures of copper oxides: (**a**) cubic Cu_2O, (**b**) monoclinic CuO, and (**c**) tetragonal Cu_4O_3. Reproduced with permission from [57].
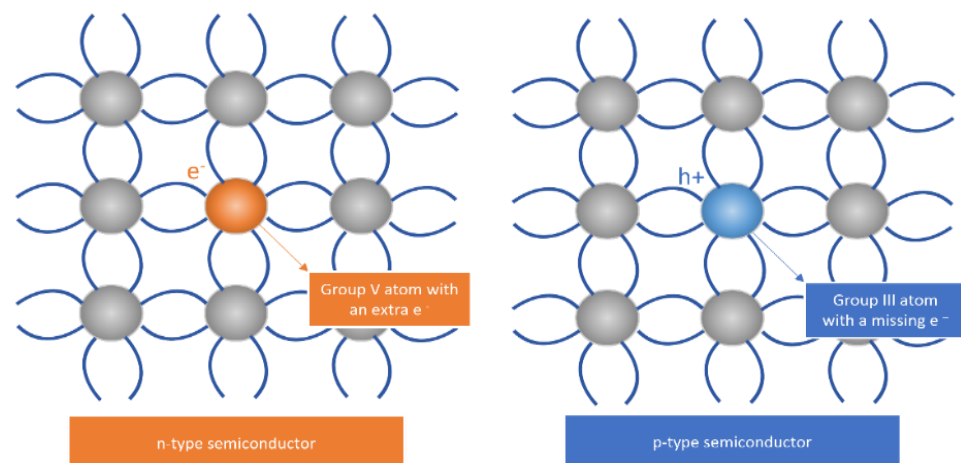
Figure 3. Difference between an n-type semiconductor and a p-type semiconductor.

2.3. Zinc Oxide

Zinc oxide is the second most abundant metal with different morphological shapes and sizes [71]. It is an inorganic multifunctional material that has favorable properties and characteristics [72]. Zinc oxide exhibits optical and piezoelectric properties that are attractive to important fields such as optoelectronics and transparent electronics [73]. It also offers a high surface area with a wide band gap of 3.37 eV, making it appropriate for photocatalysis [74]. Zinc oxides are widely used for medicinal applications since zinc is considered a dietary supplement, in addition to their antibacterial activity [75–77]. It has also been reported that the antibacterial activity of zinc oxides depends on their size and shape, which can be controlled through the synthesis route [78]. Zinc oxides can be synthesized by chemical, physical, and biological methods. These methods include microemulsion, precipitation, plasma and ultrasonic techniques, the sol–gel method, combustion, hydrothermal synthesis, and green synthesis from plants extracts [79–81]. Moreover, zinc oxides have gained attention for water purification and the removal of hazardous materials since they are biocompatible [82]. Polymorphs of zinc oxide consist of three phases shown in Figure 4: hexagonal wurtzite, cubic zinc blende, and cubic rock salt [83]. The wurtzite phase is the

most thermodynamically stable, with every zinc atom tetrahedrally coordinated with four oxygen atoms. Zinc blende and rock salt are metastable [84,85]. More zinc oxides applications include solar cells [86–88], sensors [89,90], drug delivery [91,92], and the cosmetic industry [93].
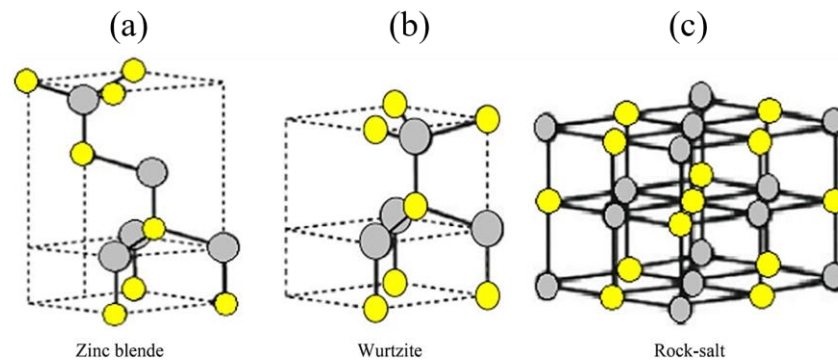
Figure 4. Polymorphs of zinc oxide: (**a**) zinc blende, (**b**) hexagonal wurtzite, and (**c**) cubic rock-salt structures. Reproduced with permission from [94].

2.4. Iron Oxide

Iron oxides have several forms which consist mainly of iron and oxygen. These forms include iron (II) oxide (wüstite, FeO), iron (II,III) oxide (magnetite, Fe_3O_4), and iron (III) oxide (ferric oxide, Fe_2O_3) [95], and are shown in Figure 5 [96]. Ferric oxide is the most common form and it has four polymorphs [97]: alpha phase hematite (α-Fe_2O_3), beta phase (β-Fe_2O_3), gamma phase maghemite (γ-Fe_2O_3), and epsilon phase (ε-Fe_2O_3) [98].
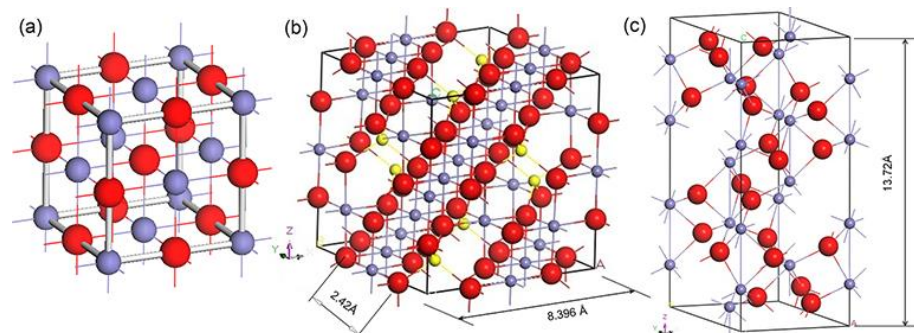
Figure 5. Forms of Iron oxides: (**a**) wüstite, (**b**) magnetite, and (**c**) Ferric oxide (hematite phase). Reproduced with permission from [96].

The magnetic properties of iron oxide NPs are highly affected by their size, dispersion, and surface [99]. Magnetite and maghemite are intrinsic ferrimagnetic materials, while hematite's magnetic properties are thermally induced [100]. The main properties that allow IONPs to be of such interest in many fields is their superparamagnetic behavior, their high surface/volume ratio, non-toxicity, reusability, biocompatibility, high stability, and resistance to change [101,102].

IONPs are also widely utilized in biomedical applications such as drug delivery systems, where the particles can be carried to a specific site with high accuracy due to the use of an external magnetic field to direct the particles [103,104]. Iron oxide NPs are usefully applied in many fields including sensing [105–107], catalysis [108–110], photodegradation [111,112], and adsorption of pollutants [113–115]. The only disadvantage in IONPs is the aggregation of particles in aqueous media, which is unfavorable in water remediation applications. Therefore, IONPs can be further stabilized by surface modification, including coating with surfactants and polymers [116,117]. For example, a study coated

iron oxide NPs with chitosan (made from chitin), which stabilized the particles and further functionalized them with amine groups, thus increasing the number of binding sites available [104].

2.5. Titanium Oxide

Titania or titanium dioxide (TiO_2) is abundant in nature and has favorable advantages with respect to energy and environmental applications [118,119]. It has been shown to be promising for these applications due to its chemical stability, biological and chemical inertness, and non-toxicity [120]. TiO_2 has long durability and transparency to visible light. It is active under UV light and functions as a semiconductor with a band gap around 3.2 eV [121]. Furthermore, titanium oxide exists in three crystalline forms, which are tetragonal anatase, tetragonal rutile, and orthorhombic brookite, with rutile being the most thermodynamically stable form [122]. Figure 6 shows the three polymorphs of titania [123]. Even though rutile is the most stable, anatase is more efficient when it comes to photocatalysis. However, some studies showed that rutile can possess good photocatalytic activity [124,125]. Anatase and rutile have tetragonal symmetry, while brookite has an orthorhombic crystalline structure [126]. The method of preparation for TiO_2 nanomaterials controls their morphology; therefore, their performance in applications can be enhanced [127]. Tailoring particle size and crystal surfaces determines which facets are exposed in TiO_2, affecting its photocatalytic activity tremendously. One of the most common methods for morphology control is the use of organic surfactants [128]. Moreover, a study synthesized different morphologies of titania by controlling the temperature in the solvothermal method [129]. Rose-like, chrysanthemum-like, and sea-urchin-like TiO_2 nanostructures (shown in Figure 7) were successfully prepared and applied for the photocatalytic degradation of Rhodamine B, where each nanostructure had a different photocatalytic performance. The applications for titania are wide, including the removal of organic pollutants [130], medical applications [131], energy storage, and sustainable energy production [132,133].
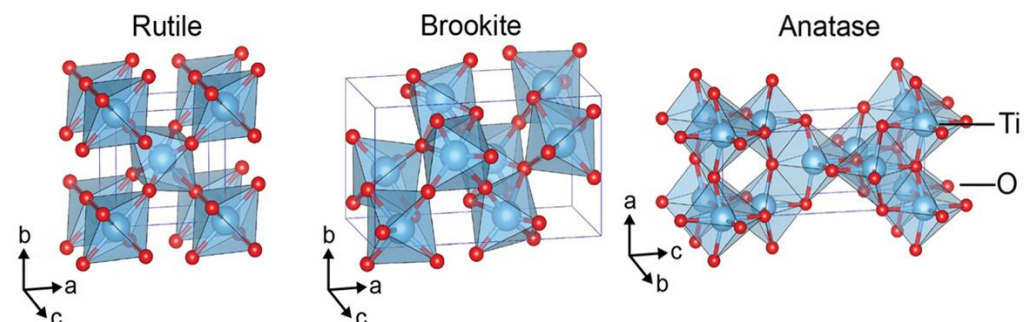
Figure 6. Polymorphs of TiO_2. Reproduced with permission from [123].
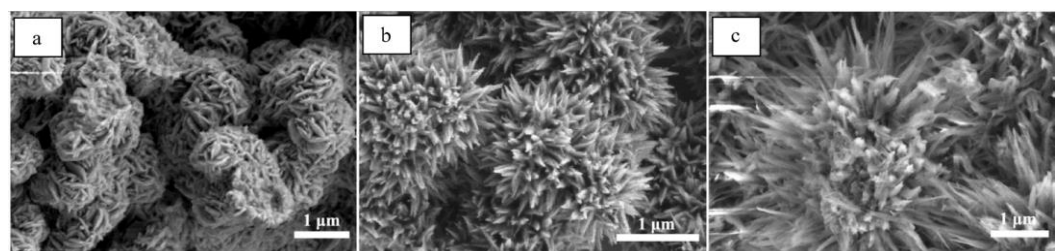
Figure 7. SEM images for TiO_2 nanostructures synthesized at (**a**) 140 °C rose-like structure, (**b**) 170 °C chrysanthemum- like structure, and (**c**) 200 °C sea-urchin-like structure. Reproduced with permission from [129].

2.6. Magnesium Oxide

Magnesium oxide (MgO) is a multifunctional inorganic material that holds great technological importance [134]. Magnesium oxide or magnesia exhibits a rock salt-type structure similar to simple NaCl [135], which is shown in Figure 8. It is known for its excellent optical, thermal, electrical, mechanical, and chemical properties [136]. Additionally, MgO has high thermal stability, with a melting point around (2852 °C) [137], and low heat capacity, making it a good insulator [138]. The particles are non-poisonous since MgO is considered an essential nutrient for plants and humans [139]. Magnesium oxides are known for their biocompatibility and stability; thus, they are frequently used in drug delivery systems and biomedical applications [140–144]. The method of synthesis of MgO highly influences the morphology and the physical structure of the nanoparticles, as in TiO_2 [145]. A study synthesized MgO nanostructures with the microwave-assisted process using two different capping agents [139]. The structures obtained were MgO nanospheres and MgO nano-cubes. The nanostructures were then used for the remediation of ciprofloxacin from aqueous solutions, and MgO nanospheres exhibited higher adsorption capacity. Moreover, MgO NPs can be fabricated by several other methods such as biosynthesis [146], ultrasound-assisted methods [147,148], sol–gel methods [149,150], pyrolysis [151], hydrothermal [152], solution combustion [153], and the co-precipitation method [154,155]. Further properties of MgO include a wide bandgap of 7.8 eV, along with high porosity and high surface area, making MgO widely applicable in many technologies [156]. The technological fields involve optoelectronics [157], enhancement of energy conversion efficiency in perovskite solar cells [158], sensors [159], superconductors [160], and toxic waste remediation [161–163]. For remediation applications, MgO nanostructures are preferred due to their nano size, which allows them to have high surface area and high surface charge [164]. Lastly, MgO nanomaterials are broadly used in the field of catalysis [165–169].
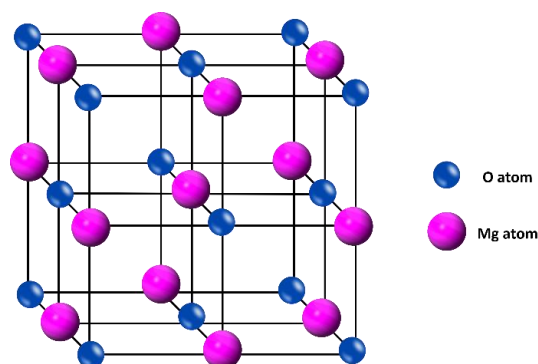
Figure 8. Rock salt-type structure of MgO.

2.7. Cerium Oxide

Cerium oxide (ceria) is a lanthanide rare earth metal oxide that attracted tremendous interest for its many applications [170]. Different types of cerium oxide nanomaterials are applied in various fields, such as biomedical fields [171–175], sensors [176,177], supercapacitors [178], fuel cells [179,180], adsorbents [181,182], photoprotective coating [183], solar cells [184], and the photodegradation of toxic pollutants [185–187]. Moreover, ceria differs from alkaline earth metals and post-transition metals due to its shielded 4f orbital electrons that affect its remarkable properties [188]. Cerium oxide has excellent chemical stability, is inexpensive, and is environmentally friendly [189]. It is highly conductive, with a large magnetic moment [190]. Cerium oxide has two oxidation states, Ce^{+3} and Ce^{+4}, where cerium (IV) is more thermally stable than the reduced version of cerium. However, cerium can switch to its other oxidation state depending on its surrounding environment [191]. Ceria's structure consists of a cubic fluorite-type oxide with many oxygen vacancies [192]. The cubic fluorite-type structure of ceria is shown in Figure 9. The surface of cerium oxide has Ce^{+3} ions as well [193]. Consequently, when cerium oxide nanoparticles (nanoceria)

are synthesized, the reactivity of nanoceria increases with the increase of Ce^{+3} ions concentration, making the NPs good for catalysis applications [194,195]. Several methods are available for the synthesis of nanoceria including the sol–gel [196], biosynthesis [197], hydrothermal [198], sonochemical [199], microwave-assisted [200], and co-precipitation [201] methods.
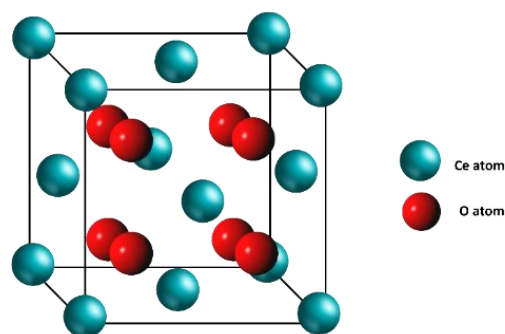
Figure 9. Cubic fluorite-type structure of CeO_2.

2.8. Aluminum Oxide

Aluminum oxide (Alumina) is a promising candidate for many applications, it is used in catalysis [202,203], insulators [204], microelectronics [205–207], sensors [208], and remediation processes [209,210]. Alumina has unique acid/base characteristics, good mechanical strength, chemical inertness towards oxidation and reduction, excellent electrical insulation, sufficient thermal stability, high surface area, and a high melting point [211,212]. Although alumina is a good insulator, F. Tzompantzi proposed that it might also be effective for photocatalytic degradation [213]. Yanet Pina-Perez proposed that the hydroxyl groups on Al_2O_3's surface might be the reason behind its photoactivity [214]. The photocatalytic activity of alumina can be increased by doping the metal ions with other metal oxides [215]. Alumina can be fabricated by various methods such as thermal decomposition [216], hydrothermal [217], combustion [218], co-precipitation [219], and sol–gel methods [220]. However, unlike other metal oxides, alumina needs high calcination temperatures (>1000 °C), which makes the fabrication costly process [221]. Alumina has many crystal structures. The most common one is α-Al_2O_3 since it is the most thermodynamically stable [222], and the structure is shown in Figure 10 [223]. Alumina has other polymorphs, including η, δ, κ, θ, γ, and ρ phases, which are metastable [224]. The type of phase produced depends highly on the method of synthesis followed. Some factors that affect the phase of alumina include the temperature, pH, pressure, and speed of stirring [225].
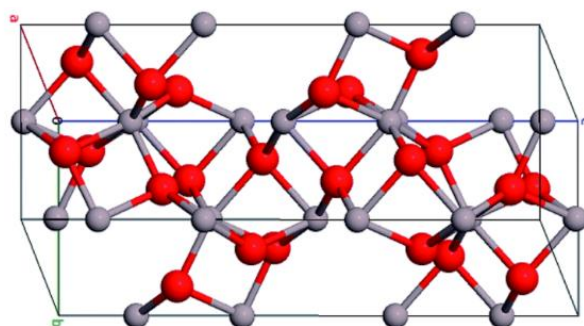
Figure 10. Rhombohedral α-Al_2O_3 structure. Reproduced with permission from [223].

2.9. Other Metal Oxides

Besides the former metal oxides discussed, several metal oxides, including MnO_2, WO_3, and NiO, have been reported for application in the remediation of pesticides from water. Manganese dioxide nanoparticles are prepared using various synthetic routes, including

hydrothermal, sol–gel, homogeneous hydrolysis, and sono-chemical methods [11,226–228]. They exist in different crystalline structures, such α-MnO$_2$ (hollandite), β-MnO$_2$ (pyrolusite), δ-MnO$_2$ (birnessite), ε-MnO$_2$ (akhtenskite), γ-MnO$_2$ (ramsdellite), λ-MnO$_2$ (defect spinels), and amorphous MnO$_2$ [229–231]. The structures of MnO$_2$ polymorphs are shown in Figure 11 [232,233]. They are widely applied as adsorbents and photocatalyst for the removal of different heavy metals and organic pollutants because they are cost effective, their structures are flexible, and they exert no toxicity [234]. Few studies were reported for the removal of pesticides using MnO$_2$ NPs. A removal percentage of 66% within 2 h was found for the photodegradation of 2,4-dichlorophenoxyacetic acid using manganese-doped zinc oxide/graphene nanocomposite under LED light [235].
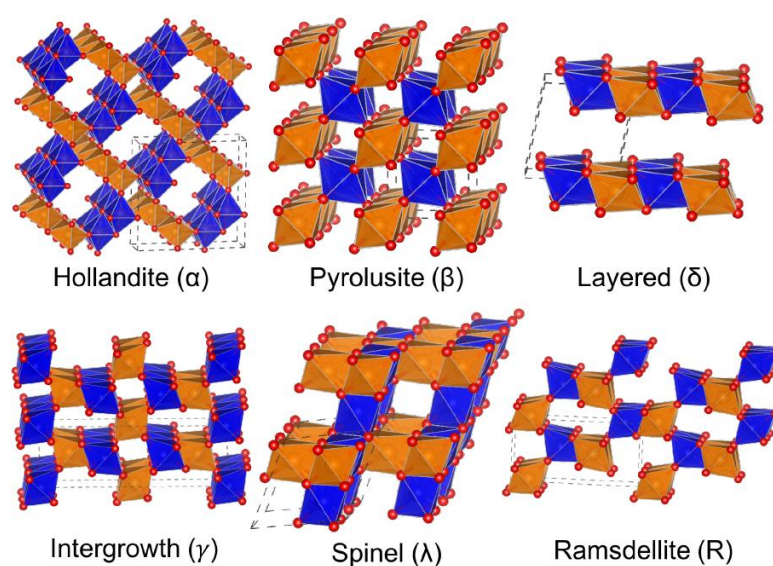
Figure 11. MnO$_2$ polymorphs. Reprinted with permission from [233]. Copyright @2018 American Chemical Society.

Various publications were considered for the fabrication of semi-conductor tungsten oxide nanoparticles using the hydrothermal method. For the remediation purposes, most of the time, tungsten oxide nanoparticles are coupled with zinc oxide and used as photocatalyst for the removal of different contaminants. This is attributed to the fact that tungsten oxide NPs have a narrow bandgap of 2.8 eV; therefore, they are weak as photocatalysts, and enhancements can be conducted by doping the material with other metals for high removal efficiency. The degradation efficiency increases with the increase in dopant percentage. At pH = 7, WO$_3$-doped ZnO NPs immobilized on glass plates show 80% removal of 2,4-dichlorophenoxyacetic acid pesticide using UV light within 2 h. Additionally, they show 99% removal of diazinon within 3 h at pH = 7 [236,237]. Figure 12 represents the effect of doping percentage on the degradation efficiency of diazinon [237].

Nickel oxide nanoparticles are hierarchical porous structures, thermally stable and with large surface area [238]. Hence, they are efficient adsorbents for different pollutants [239,240]. Nickel oxide nanoparticles are fabricated using different methods, including sol–gel [241], thermal decomposition [242], biosynthesis [243], and laser ablation [244]. A study synthesized different nanostructures of NiO using the hydrothermal method, varying the reaction temperature, time, and the molar ratios of the precursors [245]. SEM images of the synthesized nanorods, nanoplates, and nanoparticles of NiO are shown in Figure 13 [245]. Furthermore, they are p-type semiconductors with a band gap of 3.6–4.0 eV, which is sufficient for photocatalytic degradation of pesticides [246]. A layered and flower-like structure of S-doped Ni–Co LDH with uniformly dispersed spherical Fe$_3$O$_4$ NPs has shown 92% degradation of chlorpyrifos using visible light at pH = 10 within 150 min [247].
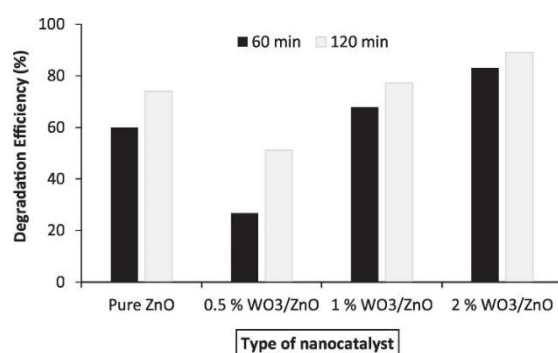
Figure 12. The effect of different dopant percentages of WO₃ZnO on the photodegradation efficiency of diazinon. Reproduced with permission from [237].
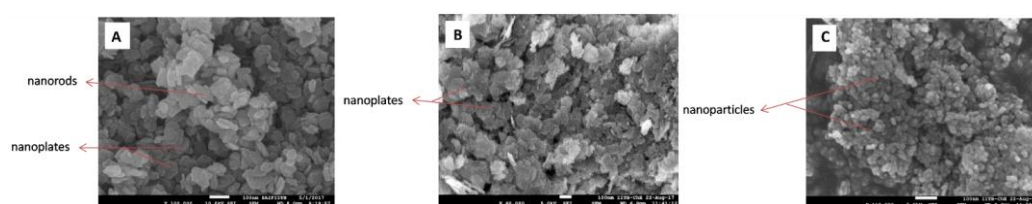
Figure 13. SEM images of NiO nanostructures synthesized with different temperatures and molar ratios of precursors; (**A**) NiO nanorods and nanoplates, (**B**) NiO nanoplates, and (**C**) NiO NPs. Reproduced with permission from [245].

2.10. Effect of Metal Oxide's Crystalline Structure on the Photocatalytic/Sorption Performance

Transition Metal oxide nanoparticles (NPs) displayed remarkable surface properties, structural characteristics, and a significant specific surface area, which made them desirable candidates for adsorption processes [22]. When the size of the molecules reduces from bulk to nanoscale, it creates an exponential increment in surface-to-volume ratio. By decreasing the size and adding active edges on organic molecules' surfaces for interaction, surface energy or adsorbent composites are improved. In contrast to their bulkier cousins, nanoparticles are far better at adsorbing organic pollutants from water. Moreover, MO NPs have lately shown a distinct potential as highly selective adsorbents intended for fast and effective removal of organic pollutants, whether used alone or in nanocomposites.

The metal oxides-based nanocomposites serve as large bandgap energy (*Eg*) semiconductors and have beneficial properties such non-toxicity and stability in water for the breakdown of organic contaminants. They also have correct structure, crystalline, and surface features. The fundamental process for the photocatalytic destruction of impurities from the surface of semiconducting materials is produced by oxygen. Oxygen vaccinations can benefit from semiconducting nanoparticles absorbing photons. By transforming organic pollutants into low/intermediate harmful yields, resulting in substances such as carbon dioxide, water, and inorganic ions, it supports environmental restoration. Once upon a time, photocatalytic treatment was thought to be the most environmentally friendly method of removing organic contaminants from wastewater. Using a short-range solar spectrum is thus a considerable obstacle to photocatalytic activity. The flaw could be fixed, for instance, by fabricating nanomaterials, doping hetero-atoms, and designing metal oxide nanocomposites through chemical and structural alterations. Worthwhile photocatalysts effectively delay electron-hole (e—h+) pair recombination, efficiently absorb the solar spectrum in the visible range, and function well as photocatalysts [248]. As photocatalysts and adsorbents, several metal oxide nanomaterials, such as Al_2O_3, CuO, CeO_2, ZnO, and TiO_2, have attracted a lot of interest [248]. To increase effectiveness and selectivity, several MO-based composites, including porous materials–reinforced metal oxides, magnetic metal oxides, metal–metal oxides, graphene–metal oxides, etc., were being studied. Adsorption events are controlled by these nanocomposites' surface properties, size, and textural char-

acteristics. Several NP morphologies provide flexible crystal defects, such as active edges on material surfaces for photocatalysis and adsorption applications.

3. Classification of Pesticides

The demand for categorizing pesticides has been raised significantly because of the increased number of pesticides, along with the variation in physical and chemical properties [249]. A considerable volume of literature has been published in this field. Recently, scientists classified pesticides based on origin and on target. Pesticides generally originate from organic, inorganic, and biological sources [250]. Table 1 elaborates on the organic class of pesticides, while Table 2 shows the classification of pesticides based on target. The pesticides' chemical structures are shown in Figure 14.

Table 1. Classification of organic pesticides based on origin.

Origin	Source	Class	Example	Features	Refs.
Organic	Natural	Plants Phytochemicals	Essential oil, plant extracts, and leftover oilseed cakes.	Low Toxicity, limited persistence in the environment, and complicated structures that prevent resistance in pests.	[251,252]
	Synthetic	Pyrethroids	Phenthion, Diazinon, Cypermethrin, Deltamethrin, Cyfluthrin, and Cypermethrin	Effect the sodium channel in insects, resulting in paralysis of the organism; highly toxic to insects and fish but less to mammals; unstable upon the exposure of light; and commonly used in food.	[253–256]
		Organophosphates	Aldrin, Dieldrin, Glyphosate, and Chlorpyrifos.	Cause paralysis, resulting in death, and dominant for variety of pests.	[257,258]
		Carbamates	Fenvalerate, Permethrin, Cyhalothrin, and Carbofuran.	Effect the nerve system of the pests, resulting in poisoning and death, and low pollution is caused upon degradation.	[259–262]
		Organochlorine	Chlorothalonil and Endrin Aldehyde.	Used for insects, long persistent in environment, affecting the nerve system and causing paralysis and death of the pests.	

Table 2. Classification of pesticides based on target.
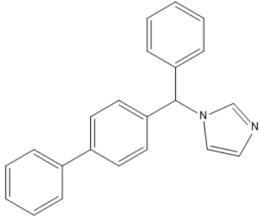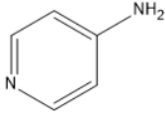
Class	Target Pests	Example	Chemical Structures	Ref.
Acaricides	Mites	Bifonazole		[250]
Avicides	Birds	Avitrol		

Table 2. *Cont.*
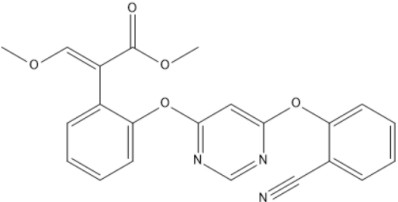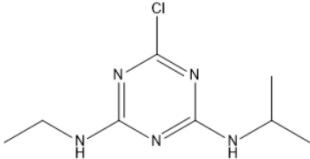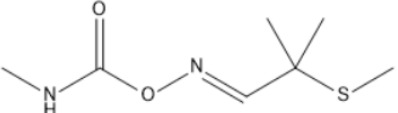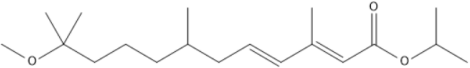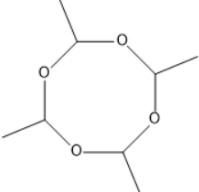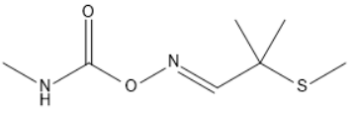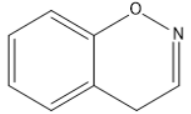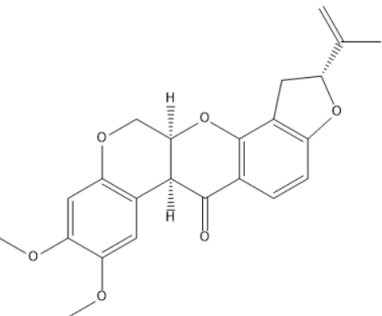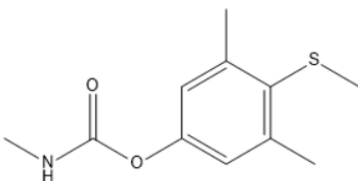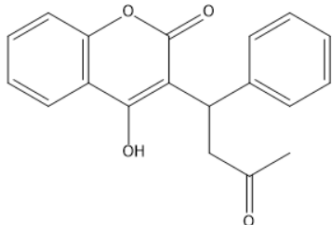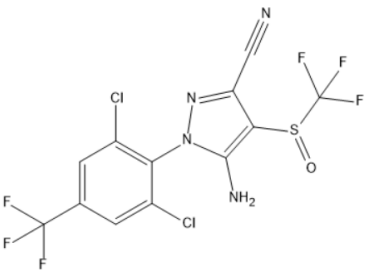
Class	Target Pests	Example	Chemical Structures	Ref.
Fungicides	Fungi	Azoxystrobin		
Herbicides	Weeds	Atrazine		
Insecticides	Insects	Aldicarb		
Larvicides	Larvae	Methoprene		
Molluscicides	Snail	Metaldehyde		
				[250]
Nematicides	Nematodes	Aldicarb		
Ovicides	Egg (prevents hatching of eggs in insects and mites)	Benzoxazine		
Piscicides	Fishes	Rotenone		
Repellents	Insects	Methiocarb		

<div align="center">Table 2. <i>Cont.</i></div>

Class	Target Pests	Example	Chemical Structures	Ref.
Rodenticides	Rodents	Warfarin		
Termiticides	Kills termites	Fipronil		[250]
Viricides	Viruses	Scytovirin		
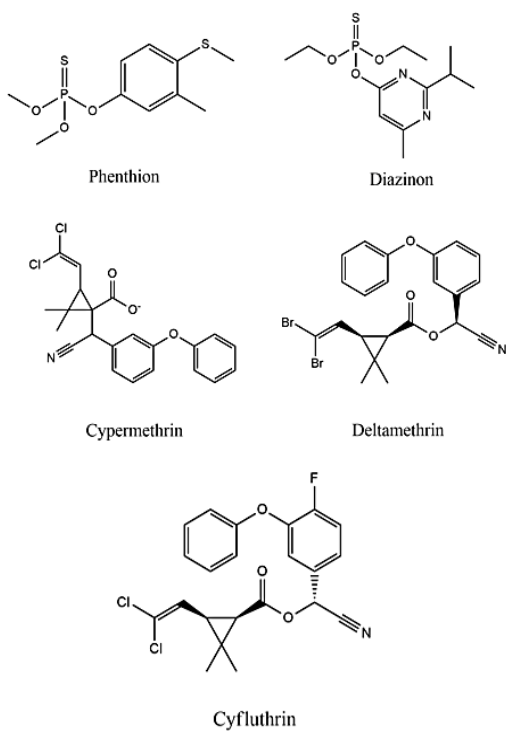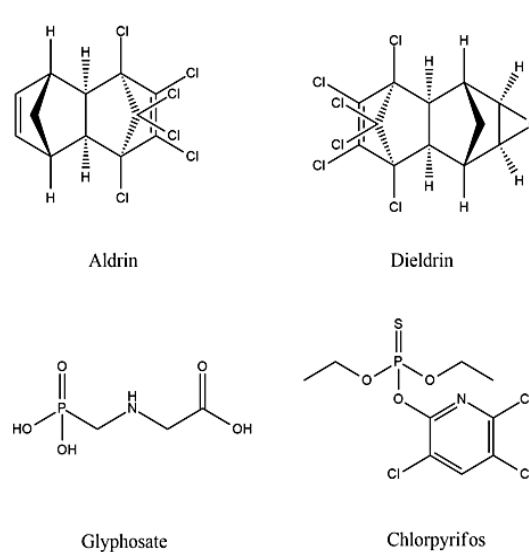
Figure 14. *Cont.*
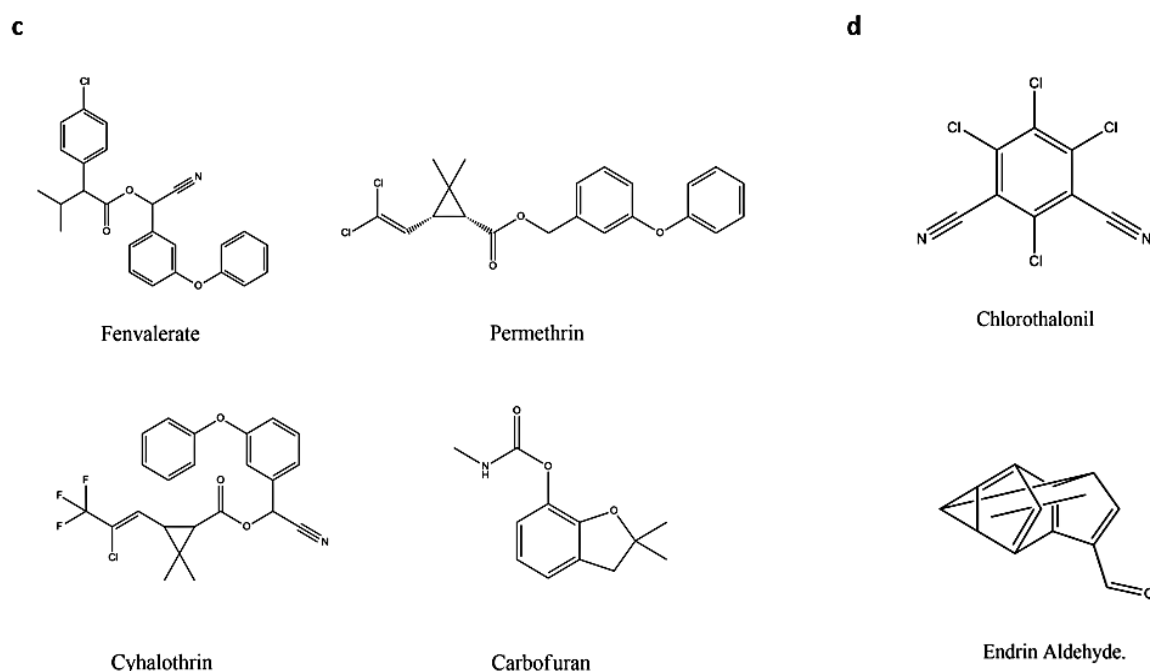
Figure 14. The chemical structures of some pesticides: (**a**) Pyrethroids, (**b**) Organophosphates, (**c**) Carbamates, and (**d**) Organochlorines.

4. Removal of Pesticides Using Functionalized Metal Oxide Nanomaterials by Adsorption

The hazards and consequences resulting from the massive use of pesticides raised the demand for efficient techniques to be employed for the removal of these contaminants. The adsorption technique has gained popularity as a simple, effective, insensitive, and flexible method [263]. It is a physiochemical method that occurs mostly in the solid–liquid form, though liquid–liquid and liquid–gas forms are also known [264–266].

In adsorption, the molecules of liquid or gases are bound to the surface of the solid. The material that provides the surface is called the adsorbent. The contaminants in the liquid or the gaseous phase are called adsorbates. Among the adsorbents reported in the literature, metal oxides have been proven as excellent adsorbents for the remediation of pesticides because of the large surface area provided for the adsorption of the pollutant [267]. The active sites and the functional groups, such as -OH, -COOH, and -C=OH, have a great impact on the efficiency of the adsorption process [268,269]. Moreover, metal oxides, having porous structures, thermal stability, low toxicity, and easy recovery, are all important for a good adsorbent. Two types of interaction between the adsorbent and the adsorbate are present: chemisorption and physisorption. Chemisorption is basically a chemical reaction between the adsorbent and the adsorbate, and it is an irreversible process. It is controlled by chemical bonds such as covalent, chelation, complex formation, proton displacement, and redox-reactions. On the other hand, physisorption, which is more dominant, is a reversible process controlled by Van der Wal's bonds, dipole–dipole attraction, and London force, etc. [270]. Table 3 provides a comparison between the types of adsorption process [271].

The adsorption process depends on various parameters that need to be optimized, including pH, temperature, time, concentration of contaminant, and sorbent dosage. Table 4 represents the adsorption capacity Q_{max} (mg/g) and the percentage removal of targeted pesticides using metal oxide nanoparticles at different parameters. The adsorption capacity is calculated in (mg/g) using the formula in Equation (1):

$$Q_{max} = \frac{C_{\circ} - C_e}{m} \times V \tag{1}$$

where C_o is the initial concentration of the pesticide (mg/L), C_e is the pesticide concentration at equilibrium (mg/L), m is the mass of adsorbent (g), and V is the volume of the solution (L).

Table 3. The advantages and disadvantages of chemisorption and physisorption.

	Physisorption	Chemisorption
Advantages	- Reversible in nature - Low adsorption enthalpy - Favors low temperature - Low activation energy	- Strong interaction between the adsorbent and the adsorbate by chemical bonds - Higher selectivity
Disadvantages	- Weak interaction between the adsorbate and the adsorbent - The extent of adsorption is inversely proportional to temperature. - Low selectivity	- Irreversible in nature - High adsorption enthalpy - Favors high temperatures - High activation energy

The adsorption isotherm and the adsorption kinetics are used to elucidate the adsorption process and to indicate the type of mechanism. The adsorption isotherm is expressed by Langmuir, Freundlich, Sips, Temkin, Redlich Peterson, Henry, and Dubinin–Astakhov (DA) models. Langmuir, Freundlich, and Dubinin–Astakhov models are most frequently used. Langmuir isotherm investigates a monolayer adsorption onto a homogeneous adsorbent, whereas Freundlich illustrates a multilayer adsorption onto a heterogeneous adsorbent. The Dubinin–Astakhov model is used to calculate the mean free adsorption energy E (J/mol). The physisorption mechanism gives an E value smaller than 8 J/mol. However, values of E from 16 J/mol to 40 J/mol indicate a chemisorption mechanism. The adsorption kinetics are equations that indicate the type of interactions between the adsorbent and the adsorbate (contaminant). Chemisorption interaction is described by a pseudo-second-order equation. The pseudo-first-order equation is applied for the physisorption interaction [272,273].

Despite the advantages of adsorption, there is one certain drawback associated with the use of this technique: it produces secondary pollutants which require highly advanced procedures for recycling and decomposing for them to be used in the industrial field [22].

Table 4. Adsorptive remediation of pesticides using metal oxides NPs.

Adsorbent [a]	Targeted Pesticides [b]	Target Operation Parameters						Adsorption Modelling			Q_max (mg/g) or Percentage Removal (%)/Percentage Recovery	Ref.
		Pesticide Conc.	Adsorbent Dosage (g) or g/L	pH	Temp. (K)	Time (min)	Kinetics [c]	Isotherm [d]	Mechanism [e]			
Co_3O_4/G-MCM-41	Methyl parathion	-	-	-	-	-	PFO, PSO	L, F, DA	-		175.2	[274]
NiO/Co@C	Chlorothalonil	0.045 g/L	0.01 g	-	-	15	PSO	L	π-CM, H		62.2	[275]
	Tebuconazole	0.045 g/L	0.01 g	-	-	15	PSO	L	π-CM, H		40.5	
	Chlorpyrifos	0.045 g/L	0.01 g	-	-	15	PSO	L	π-CM, H		60.3	
	Butralin	0.045 g/L	0.01 g	-	-	15	PSO	L	π-CM, H		50.2	
	Deltamethrin	0.045 g/L	0.01 g	-	-	15	PSO	L	π-CM, H		54.1	
	Pyridaben	0.045 g/L	0.01 g	-	-	15	PSO	L	π-CM, H		51.3	
CeO_2	2,4-Dichlorophenoxyacetic acid	0.01 g/L	0.025 g	-	308	120	PSO	L, F, S	π–π, e⁻		95.78	[276]
Fe_3O_4@ZnAl-LDH@MIL-53(Al)	Triadimefon	5.0–600 mg kg⁻¹	30 g/L	6	308.15	5	PSO	L	π–π, H, C, (π-CM), P		46.08	[277]
$MgFe_2O_4$	Chlorpyrifos	20 mg/L	0.01 g/L	10	295	360	PSO	L	-		4461	[278]
Fe_3O_4	Atrazine	50 mg/L	0.1 g	2	298	55	PFO	L	-		77.5	[279]
	Methoxychlor	50 mg/L	0.1 g	2	298	55	PFO	L	-		163.9	
ZnO	Naphthalene	25 mg/L	0.012 g	4	298	40	PSO	L, F, T	-		66.8	[280]
CTAB-ZnO	Naphthalene	25 mg/L	0.08 g	4	298	40	PSO	L, F, T	-		89.96	
BMTF-IL-ZnO	Naphthalene	25 mg/L	0.06 g	4	298	40	PSO	L, F, T	-		148.3	
$ZnO/ZnFe_2O_4$	Atrazine	50 mL aq. solution	0.4 g/L	7	298	4320	-	D.A	π–π, H, h, e-		-	[281]
Fe_3O_4@SiO_2@GO-2-phenylethylamine	Chlorpyrifos	10 mL aq. Solution	0.015 g	7	298	15	PSO	S	π–π, H		88%	[32]
	Malathion	10 mL aq. Solution	0.015 g	7	298	15	PSO	S	H		76%	
	Parathion	10 mL aq. Solution	0.015 g	7	298	15	PSO	S	π–π, H		85%	
Fe_3O_4/MOF-99	Dinotefuran	0.3–1.5 ng/mL	0.015 g	-	-	20	-	-	π–π		88–107%	[282]
	Thiamethoxam	0.3–1.5 ng/mL	0.015 g	-	-	20	-	-	π–π		88–107%	

Table 4. *Cont.*

Adsorbent [a]	Targeted Pesticides [b]	Target Operation Parameters						Adsorption Modelling				Ref.
		Pesticide Conc.	Adsorbent Dosage (g) or g/L	pH	Temp. (K)	Time (min)	Kinetics [c]	Isotherm [d]	Mechanism [e]	Q_{max} (mg/g) or Percentage Removal (%)/Percentage Recovery	
Fe_3O_4@SiO_2@MOF/TiO_2	Triadimenol	0.001 g/L	0.04 g	7	298–313.15	1–60	PSO	-	π–π	90.2–104%	[283]
	Hexaconazole	0.001 g/L	0.04 g	7	298–313.15	1–60	PSO	-	π–π	90.2–104%	
	Diniconazole	0.001 g/L	0.04 g	7	298–313.15	1–60	PSO	-	π–π	90.2–104%	
Fe_3O_4-GO@MOF-199.	Flusilazole	0.002 g/L	0.02 g	-	-	15	-	-	h, π–π, H, e^-	0.0356	[284]
	Fenbuconazole	0.002 g/L	0.02 g	-	-	15	-	-	h, π–π, H, e^-	0.0342	
	Myclobutanil	0.002 g/L	0.02 g	-	-	15	-	-	h, π–π, H, e^-	0.0324	
Fe_3O_4–MWCNTs-ZIF-8	Triazophos	0.015 g	0.002–0.08 g/L	4	RT	15	-	F	-	3.12	[285]
	Diazinon	0.015 g	0.002–0.08 g/L	4	RT	15	-	F	-	2.59	
	Phosalone	0.015 g	0.002–0.08 g/L	4	RT	15	-	F	-	3.80	
	Profenofos	0.015 g	0.002–0.08 g/L	4	RT	15	-	F	-	3.89	
	Methidathion	0.015 g	0.002–0.08 g/L	4	RT	15	-	F	-	2.34	
	Ethoprop	0.015 g	0.002–0.08 g/L	4	RT	15	-	F	-	2.18	
	Sulfotep	0.015 g	0.002–0.08 g/L	4	RT	15	-	F	-	2.84	
	Isazofos	0.015 g	0.002–0.08 g/L	4	RT	15	-	F	-	3	
Chitosan–CuO	Thiophanate-methyl	0.1 g/L	0.1 g	7	RT	25	-	L, F	h	250	[286]
	Methomyl	0.1 g/L	0.1 g	7	RT	25	-	L.F	-	20	
	Malathion	0.02 g/L	1 g/L	2	303	960	PSO	L, F	-	322.6	
Chitosan-ZnO	Thiophanate-methyl	0.1 g/L	0.1 g	7	RT	25	-	L, F	h	100	
	Methomyl	0.1 g/L	0.1 g	7	RT	25	-	L, F	-	10	
Fe_3O_4/CuO/Activa-ted carbon	Permethrin	0.0001 g/L	0.5 g	7	298	90	-	-	-	99%	[287]
	Imidacloprid	0.01 g/L	0.02 g	7	298	10	PSO	F	C	99%	[288]
ZnO-IPPs	Chlorpyrifos	0.01–0.6 g/L	0.03 g	2	303–323	30	PSO	L, F, T, D. A	-	47.846	[289]
ZnO-CP	Metribuzin	0.033–0.155	0.08 g	3	303–363	80	PSO	F	-	200	[290]

Table 4. *Cont.*

Adsorbent [a]	Targeted Pesticides [b]	Target Operation Parameters						Adsorption Modelling				Ref.
		Pesticide Conc.	Adsorbent Dosage (g) or g/L	pH	Temp. (K)	Time (min)	Kinetics [c]	Isotherm [d]	Mechanism [e]	Qmax (mg/g) or Percentage Removal (%)/Percentage Recovery	
MOM-Fe$_3$O$_4$	Triclosan	0.005–0.2 g/L	0.01–0.05 g/L	4, 7, 10	293, 303, 313	600	PFO	L	-	103.45	[291]
N-NiO@N-Fe$_3$O$_4$@N-ZnO	Atrazine	0.04 g/L	0.1 g	5	-	80	PSO	L	-	92%	[292]
MgAl$_2$O$_4$	Dimethomorph	-	0.5–2 g	5.5	-	10	-	-	-	% Recovery = 90–94%	[293]
Fe$_3$O$_4$ @PS	Lindane	2, 10, 50, 200 μg/L	0.02 g/L	-	RT	<20	PSO	L	-	10.2	[294]
	Aldrin	2, 10, 50, 200 μg/L	0.02 g/L	-	RT	<20	PSO	L	-	24.7	
	Dieldrin	2, 10, 50, 200 μg/L	2×10^{-5} g/L	-	RT	<20	PSO	L	-	21.3	
	Endrin	2, 10, 50, 200 μg/L	2×10^{-5} g/L	-	RT	<20	PSO	L	-	33.5	
MgO	Diazinon	0.30 g/L	0.05 or 0.10 g	-	-	<5	-	-	-	21–37%	[295]
	Fenitrothion	0.28 g/L	0.05 or 0.10 g	-	-	5–60	-	-	-	27–47%	
Fe$_3$O$_4$@nSiO$_2$@mSiO$_2$	DDT	0.0015 g/L	0.05 g	-	-	15	PSO	-	-	94%	[296]

RT = room temperature; [a] Adsorbent: ZnONPs-IPPs = zinc oxide nanoparticles-impregnated pea peels; MOM-Fe$_3$O$_4$ = functionalized iron oxide nanoparticles with Moringa oleifera Lam. seeds; Fe$_3$O$_4$ @PS = magnetic nanosphere coated by polystyrene; ZnO-CP = zinc oxide with cucumber peel; CTAB-ZnO = cetyltrimethylammonium bromide functionalized zinc oxide; BMTF-IL-ZnO = 1-Butyl-3-methylimidazolium tetrafluoroborate functionalized zinc oxide; Hr-MgO = hierarchical magnesium oxide; [b] targeted pesticides fenitrothion = dimethoxy-(3-methyl-4-nitrophenoxy)-thioxophosphorane; DDT = dichloro-diphenyl-trichloroethane; Diazinone = diethoxy-[(2-isopropyl-6- methyl-4-pyrimidinyl)oxy]-thioxophosphorane; [c] Kinetic equation; PSO = pseudo-second order; PFO = pseudo-first order; [d] Isotherm equation; L = Langmuir; F = Freundlich; S = Sips; T = Temkin; DA = Dubinin–Astakhov; [e] Mechanisms: electrostatic interaction (e$^-$), hydrophobic interaction (h), π–π interaction (π–π), π-complex formation with cations (including metal or positive ion charge groups) (π-CM), hydrogen bond interaction (H), coordination or covalent bond (C).

5. Removal of Pesticides Using Functionalized Metal Oxide Nanomaterials by Photocatalytic Degradation

Photocatalytic degradation is an advanced oxidation process that destroys toxic substances into other harmless products. Unlike other remediation techniques, photocatalytic degradation completely mineralizes the toxicant, without the production of secondary waste [36]. The mechanism of photocatalytic degradation starts when the photocatalyst is irradiated under UV or visible light that has energy equal to or greater than its band gap [297]. The detailed mechanism of the reaction is shown in Equation (2) to Equation (8). Notably, photocatalytic degradation of organic molecules is carried out in a similar manner [21]. When the photocatalyst is irradiated, electrons are excited from the valence band of the photocatalyst to the conduction band generating electron/hole pairs (e^-/h^+), as seen in Equation (2).

Oxygen in water becomes attracted to the positive holes generated by the radiation, and a proton leaves the water molecule, leaving hydroxyl ions adsorbed on the surface, which is shown in Equation (3). It is noted that *X resembles a species absorbed into the hole. Electrons act as reducing agents while positive holes act as oxidizing agents. Electrons reduce the oxygen adsorbed on the surface of the photocatalyst, generating a superoxide radical in Equation (4). Then, a superoxide and a proton react to produce a peroxide radical that is still adsorbed on the surface, and a hydrogen transfer from two peroxides occurs to produce hydrogen peroxide and oxygen (Equations (5) and (6)). Finally, hydrogen peroxide is irradiated to produce hydroxyl radicals in Equation (7), and hydroxyl radicals degrade the organic pesticide to water, carbon dioxide, and other products, depending on the type of pesticide (Equation (8)). Figure 15 illustrates a schematic mechanism for the photodegradation of a pesticide [298].

$$\text{photocatalyst} + hv \rightarrow \text{h}^+ + \text{e}^- \tag{2}$$

$$\text{h}^+ + \text{H}_2\text{O} \rightarrow \text{*OH} + \text{H}^+ \tag{3}$$

$$\text{*O}_2 + \text{e}^- \rightarrow \text{*O}_2^- \tag{4}$$

$$\text{*O}_2^- + \text{H}^+ \rightarrow \text{*OOH} \tag{5}$$

$$2\text{*OOH} \rightarrow \text{*O}_2 + \text{H}_2\text{O}_2 \tag{6}$$

$$\text{H}_2\text{O}_2 + hv \rightarrow 2\,^{\cdot}\text{OH} \tag{7}$$

$$\text{Pesticide} + {}^{\cdot}\text{OH} \rightarrow \text{intermediates} \rightarrow \text{H}_2\text{O} + \text{CO}_2 \tag{8}$$
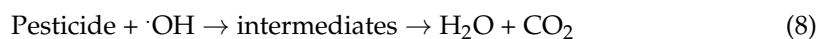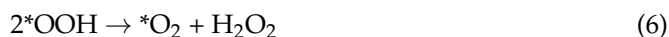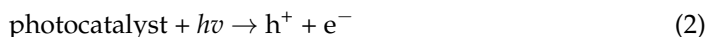
Finding the optimum conditions for photocatalysis is extremely important to achieve maximum efficiency of degradation. The recent studies reporting on the photodegradation of different types of pesticides by metal oxide nanomaterials and their composites under UV or visible light have been cited in Table 5. The conditions that correspond to the maximum efficiency of degradation in the studies have been reported.

Several parameters should be considered when carrying out photocatalytic degradation [248]. The nature and type of the photocatalyst, concentration of the photocatalyst, concentration of the pesticide, pH, and irradiation time. Surface morphology, agglomeration, and size affect the behavior of the photocatalyst during the process. Moreover, the higher the concentration of the photocatalyst, the more efficient the degradation [299]. This is a result of having more active sites on the surface of the photocatalyst, thus generating more electron/hole pairs and, consequently, more hydroxyl radicals. However, it is worth mentioning that after very high dosages of the photocatalyst, the efficiency of the reaction

decreases due to the blockage of light penetration [300]. Concerning the concentration of the pesticide, at high dosages of the pollutant, most studies reported a decrease in the efficiency of degradation, as reported in Table 4. Increasing the dosage of the pesticide allows for the adsorption of the pesticide on the active sites of the catalyst, preventing the generation of hydroxyl radicals [301]. Depending on the structure of both pesticide and the nano-photocatalyst, the pH can affect the reaction behavior between them. The reaction will be favorable in the pH that allows for the attraction of the photocatalyst and the pesticide, as well as the accelerated production of hydroxyl radicals [302]. The effect of irradiation time is directly proportional to the efficiency of degradation. The increase of irradiation time permits more excitation to occur, and consequently, more radicals are formed [303].
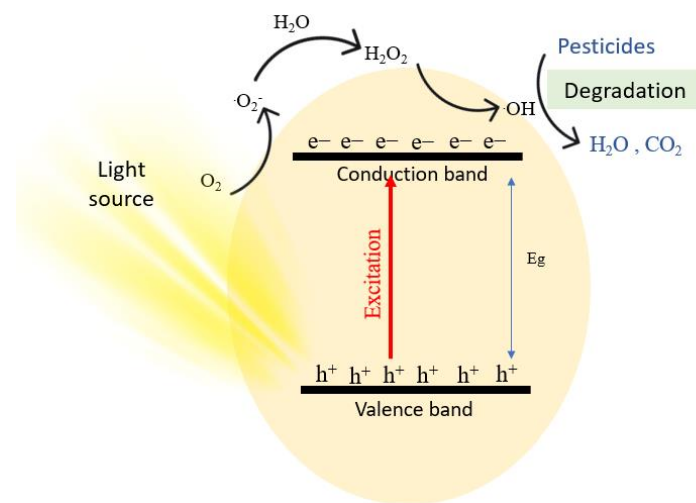
Figure 15. A schematic mechanism for the photodegradation of a pesticide.

Metal oxide semiconductors, such as ZnO and TiO_2 nanomaterials, are the most appropriate for photocatalytic degradation (Table 4) [298]. This is attributed to the fact that they can produce electron/hole pairs (e^-/h^+) more when irradiated with light. Most photocatalysis research focuses on TiO_2 nanomaterials [304–306]. The problem with ZnO NPs is the fast recombination of the generated electron/holes [301]. However, recently, it has been discovered that doping the semiconductors with other metals, or further functionalizing them, leads to better separation of charges [307].

Table 5. Reported studies for the photodegradation of pesticides by metal oxide nanomaterials and their composites.

Photocatalyst	Structure	Target Pesticide	Light Source	Conc. of Pollutant	Conc. of Photocatalyst	Irradiation Time (min)	pH	Degradation Efficiency (%)	Ref.
Co_3O_4/MCM-41 NPs	MCM-41 nanospheres decorated Co_3O_4.	methyl parathion	visible	100 mg/L	0.25 g	90	8	100	[274]
MCM-41/Co_3O_4 nanocomposite	Spherical shape.	acephate	visible	100 mg/L	0.25 g	70	8	100	[308]
Co_3O_4/MCM-41 nanocomposite	MCM-41 spherical grains decorated by Co_3O_4 NPs.	omethoate	visible	50 mg/L	0.25 g	30	>6.5	100	[309]
Cu/ZnO nanocomposite	Spherical and elliptical.	monocrotophos	visible	0.5 L	0.5 g	180	7	~90	[310]
CuO/TiO_2/PANI nanocomposite	CuO/TiO_2 spherical NPs embedded in tubular PANI.	chlorpyrifos	visible	5 mg/L	45 mg	90	7	95	[35]
ZnO/CuO nanocomposites	Shape depends on the synthesis conditions.	triclopyr	UV	10 mg/L	0.10 g/150 mL	100	4	100	[311]
CuO NPs	Spherical and flower-like shape.	lambda-cyhalothrin	UV	10 mg/L	3 mg/L	180	7	99	[312]
NiO NPs	Spherical and flower-like shape.	lambda-cyhalothrin	UV	10 mg/L	4 mg/L	180	7	89	[312]
Cu_2O/$BiVO_4$ composites	Shape depends on the synthesis conditions.	4-chlorophenol	visible	50 mg/L	5 g/L	240	-	44	[313]
Mn-doped zinc oxide/graphene nanocomposite	Spherical particles distributed onto graphene sheets.	2,4-dichlorophenoxyacetic acid	LED	25 mg/L	2 g/L	120	5	66.2	[235]
WO_3 doped ZnO NPs immobilized on glass plates	Heterogenous surface.	2,4-dichlorophenoxyacetic acid	UV	25 mg/L	-	120	7	80	[236]
Nano hydroxyapatite modified CFGO/ZnO nanorod composite	A complex porous surface.	chlorpyrifos	visible	5 mg/L	0.1 g	30	3	100	[302]

Table 5. *Cont.*

Photocatalyst	Structure	Target Pesticide	Light Source	Conc. of Pollutant	Conc. of Photocatalyst	Irradiation Time (min)	pH	Degradation Efficiency (%)	Ref.
WO_3 doped ZnO NPs immobilized on glass plates	Heterogenous surface.	diazinon	UV	10 mg/L	10 mg/cm^2	180	7	99	[237]
ZnO/rGO nanocomposite	rGO film with agglomerations of ZnO nanosheets.	dimethoate	UV	5 mg/L	50 mg	180	-	~99	[301]
ZnO NPs	Spherical.	monocrotophos	UV	500 mL aq. solution	2 g	120	4	88	[314]
ZnO NPs	-	methyl parathion	UV	-	85 mg/L	100	>9	~70	[315]
ZnO NPs	-	parathion	UV	-	85 mg/L	100	>9	~65	[315]
Cu-doped ZnO nanorods	Nanorods.	diazinon	UV	20 mg/L	0.2 g/L	120	7	96.97	[36]
ZnO nanorods nanorod incorporated carboxylic GR/PANI composite	A complex porous surface.	diuron	visible	5 mg/L	0.1 g	40	3.0	100	[316]
Fe-ZnO nanocomposite	Rough surface due to Fe ions doped in ZnO.	chlorpyrifos	UV	10 mg/L	25 mg/L	60	-	93.5	[317]
Ag-ZnO nanocomposite	Uniform distribution of Ag onto ZnO surfaces.	chlorpyrifos	Sunlight	50 mg/L	20 mg	40	-	~90	[318]
TiO_2 NPs	Aggregated semi-spherical.	imidacloprid	UV	100 mg	100 mg/L	20	7.5	88.15	[319]
ZnO NPs	Aggregated semi-spherical.	imidacloprid	UV	100 mg	100 mg/L	20	7.5	~80	[319]
$rGO/Fe_3O_4/ZnO$ ternary nanohybrid	A complex layered surface.	metalaxyl	visible	10 mg/L	0.5 g/L	120	7	92.11	[320]
La-ZnO-PAN fibers	La and ZnO embedded on PAN nanofibers.	methyl parathion	UV	10 mg/L	50 mg/L	150	<3	100	[321]
La-ZnO-PAN fibers	La and ZnO embedded on PAN nanofibers.	atrazine	UV	10 mg/L	30 mg/L	60	7	98	[299]

Table 5. *Cont.*

Photocatalyst	Structure	Target Pesticide	Light Source	Conc. of Pollutant	Conc. of Photocatalyst	Irradiation Time (min)	pH	Degradation Efficiency (%)	Ref.
rGO/ZnO nanocatalyst	ZnO NPs uniformly distributed on rGO nanosheets.	metalaxyl	UV	10 mg/L	0.75 g/L	120	7	90.25	[322]
Cu-ZnO nanocomposite	Cu loaded on ZnO nanorods.	methyl parathion	UV	500 mg/L	20 mg/L	80	-	99	[323]
ZnO/CeO$_2$ nanocomposite	CeO$_2$ NPs loaded onto ZnO hexagonal nano-carrots.	triclopyr	UV	150 mL aq. solution	100 mg	70	7	83.24	[324]
ZnO nanofilms	Nanoflowers.	temephos	Sunlight simulator	10 mg/L	-	12	-	100	[325]
Fe/Ag@ZnO nanostructures	Nanoflowers.	2,4-dichlorophenoxyacetic acid	UV/visible	62 mg/L	0.078 g/L	63	5	80	[326]
ZnO/TiO$_2$-Fe$_3$O$_4$ nanocomposite	Fe$_3$O$_4$ and TiO$_2$ uniformly distributed on the porous nanostructure of ZnO.	chlorpyrifos	visible	8 mg/L	60 mg	50	10	94.8	[327]
PANI/ZnO-CoMoO$_4$ nanocomposite	Spherical CoMoO$_4$ and ZnO NPs distributed on PANI.	imidacloprid	visible	4.5 mg/L	163.5 mg	180	4	97	[328]
Ag@ZnO nano-stars	Star-like shape.	methyl parathion	visible	0.01 mg/L	25 mg	200	7	-	[329]
Pd@ZnO nano-stars	Star-like shape.	methyl parathion	visible	0.01 mg/L	25 mg	200	7	-	[329]
Cu-ZnO nano heterojunction particles	Cu NPs embedded onto ZnO surface.	chlorpyrifos	sunlight	200 mg/L	250 mg	240	6	91	[330]
Li dope ZnO nanostructures	Aggregated spherical NPs.	triclopyr	UV	100 mL aq. solution	1 g/L	120	7	~50	[331]
ZnO@CdS nanostructures	CdS aggregated spherical NPs and ZnO nanoflowers.	chlorpyrifos	sunlight	2 mg/L	25 mg/L	360	7	91	[300]

Table 5. *Cont.*

Photocatalyst	Structure	Target Pesticide	Light Source	Conc. of Pollutant	Conc. of Photocatalyst	Irradiation Time (min)	pH	Degradation Efficiency (%)	Ref.
ZnO@CdS nanostructures	CdS aggregated spherical NPs and ZnO nanoflowers.	atrazine	sunlight	50 mg/L	20 mg/L	360	7	89	[300]
MgO NPs immobilized on concrete	MgO NPs immobilized on concrete surface.	diazinon	UV	5 mg/L	-	120	7	99.46	[332]
$CeO_2/TiO_2/SiO_2$ nano-catalyst	Nearly spherical	chlorpyrifos	UV	2 mg/L	0.21 g/L	90	5.4	81.1	[333]
CeO_2-SiO_2 NPs	-	chlorpyrifos	UV	10 mL aq. solution	7 mg	150	9	~90	[334]
Fe doped CeO_2-SiO_2 nanocomposite	Spherical NPs	chlorpyrifos	UV	20 mg/L	7 mg	~230	-	81.31	[335]
$GO/Fe_3O_4/TiO_2$-NiO nanocomposite	Spherical Fe_3O_4, TiO_2, NiO dispersed on GO nanosheets.	imidacloprid	visible	5 mg/L	0.08 g	45	9	97.47	[303]
Au/Fe_3O_4 core/shell NPs	Spherical	malathion	UV	10 mg/L	10^{-4} mol/L	90	-	76	[336]
S-doped Ni–Co LDH/Fe_3O_4 nanocomposite	A layered and flower-like structure with uniformly dispersed spherical Fe_3O_4 NPs.	chlorpyrifos	visible	2.5 mg/L	60 mg	150	10	92.5	[247]
KIT-5/Bi_2S_3-Fe_3O_4 nanocomposite	Spherical Bi_2S_3 and Fe_3O_4 NPs uniformly distributed on 3-D mesoporous cubic KIT-5 surface.	parathion	visible	4.5 mg/L	55 mg	55	8	98.7	[337]
GO- Fe_3O_4/TiO_2 nanocomposite	Fe_3O_4 NPs and mesoporous TiO_2 dispersed uniformly on GO nanosheets.	chlorpyrifos	visible	5 mg/L	100 mg	60	~8	97	[304]

Table 5. *Cont.*

Photocatalyst	Structure	Target Pesticide	Light Source	Conc. of Pollutant	Conc. of Photocatalyst	Irradiation Time (min)	pH	Degradation Efficiency (%)	Ref.
KIT-6/WS$_2$-Fe$_3$O$_4$ nanocomposite	Spherical WS$_2$ and Fe$_3$O$_4$ NPs uniformly distributed on 3-D mesoporous cubic KIT-6 surface.	chlorpyrifos	visible	7.2 mg/L	50 mg	52	6	92.1	[338]
Fe$_3$O$_4$/CdS–ZnS nanocomposite	Spherical CdS, Fe$_3$O$_4$ and ZnS NPs.	chlorpyrifos	visible	10 mg/L	0.01 g	60	7	94.55	[339]
Fe$_3$O$_4$@WO$_3$/SBA-15 nanocomposite	Agglomerates of WO$_3$ nanoplates on Fe$_3$O$_4$ NPs and uniform rods of hexagonal SBA-15.	2,4-dichlorophenoxyacetic acid	UV	10^{-6} mol/L	40 mg	240	-	90.73	[340]
TNP-Pd-Fe$_3$O$_4$/GO photocatalyst	Fe$_3$O$_4$ NPs, Pd, and TiO$_2$ nanoplates were dispersed uniformly on GO sheets.	parathion	visible	10 mg/L	80 mg	40	10	98.5	[341]
BiOBr/Fe$_3$O$_4$ photocatalyst	Agglomerated Fe$_3$O$_4$ NPs deposited on BiOBr microspheres.	glyphosate	visible	100 mg/L	0.08 g	60	-	97	[342]
Ag$_2$S doped nanostructures of Fe$_3$O$_4$ @Ag$_3$PO$_4$ ultrathin films	Ag$_2$S and Fe$_3$O$_4$ NPs doped on Ag$_3$PO$_4$ ultrathin film.	imidacloprid	visible	2 mg/L	30 mg	90	4.3–9	98.9	[343]
Ag$_2$S doped nanostructures of Fe$_3$O$_4$ @Ag$_3$PO$_4$ ultrathin films	Ag$_2$S and Fe$_3$O$_4$ NPs doped on Ag$_3$PO$_4$ ultrathin film.	thiacloprid	visible	2 mg/L	30 mg	60	-	90	[343]
g-C$_3$N$_4$/Cu/TiO$_2$ nanocomposite	Cu and TiO$_2$ NPs dispersed on the irregular layered structure of graphitic-C$_3$N$_4$.	endosulfan	visible	5 mg/L	40 mg	80	6.8	60	[344]
SBA-15/TiO$_2$ nanocomposite	TiO$_2$ NPs dispersed on the hexagonal array of SBA-15.	trifluralin	UV	60 mg/L	0.2 g/L	30	10	90	[345]

Table 5. *Cont.*

Photocatalyst	Structure	Target Pesticide	Light Source	Conc. of Pollutant	Conc. of Photocatalyst	Irradiation Time (min)	pH	Degradation Efficiency (%)	Ref.
SBA-15/TiO$_2$ nanocomposite	TiO$_2$ NPs dispersed on the hexagonal array of SBA-15.	pendimethalin	UV	60 mg/L	0.2 g/L	30	10	82.5	[345]
TiO$_2$ NPs	Irregular agglomerated NPs.	imidacloprid	UV	5 mg/L	0.6 g/L	300	6.35	99	[305]
TiO$_2$ nanostructures modified with Cu	Homogenous nano-porous structure of TiO$_2$ with Cu dispersed on the surface.	imidacloprid	UV/vis	25 mg/L	-	60	-	-	[306]
TiO$_2$/CNT/Pd photocatalyst	Heterostructure spherical Pd-doped TiO$_2$ nanoparticles on carbon nanotubes.	neonicotinoids thiacloprid	sunlight	5 mg/L	0.1 g/L	180	7	100	[346]
TiO$_2$/CNT/Pd photocatalyst	Heterostructure spherical Pd-doped TiO$_2$ nanoparticles on carbon nanotubes.	imidacloprid	sunlight	5 mg/L	0.1 g/L	180	7	99.8	[346]
TiO$_2$/CNT/Pd photocatalyst	Heterostructure spherical Pd-doped TiO$_2$ nanoparticles on carbon nanotubes.	clothianidin	sunlight	5 mg/L	0.1 g/L	180	7	100	[346]
TiO$_2$ nanoparticles	Spherical with only a small quantity of hexagonal diameters.	dimethoate	UV	5 mg/L	300 mg/L	320	-	100	[347]
TiO$_2$ nanoparticles	Spherical with only a small quantity of hexagonal diameters.	methomyl	UV	5 mg/L	300 mg/L	320	-	100	[347]
CuS/TiO$_2$ (CuST) nanoparticles	Coalesced and form a textured/porous nanostructure.	4-chlorophenol	UV	20 mg/L	100 mg	150	-	87	[348]
Pt@TiO$_2$/rGO nanocomposite	Monodisperse quasi-spherical Pt@TiO$_2$ NPs deposited on the rGO nanosheets.	diuron	UV	0.03 mmol/L	7 mg	-	7	100	[349]

Table 5. *Cont.*

Photocatalyst	Structure	Target Pesticide	Light Source	Conc. of Pollutant	Conc. of Photocatalyst	Irradiation Time (min)	pH	Degradation Efficiency (%)	Ref.
(CMC/Tryp/TiO$_2$).	Platelet-like crystallites.	2,4-dichlorophenol	UV	200 mg/L	0.5 g/L	-	-	-	[350]
SBA-16/TiO$_2$ nanocomposites	Rutile phase.	commercial paraquat (PQ) herbicide	UV	50 mg/L	100 mg in 250 mL aq. Solution	1440	-	70	[351]
Ce-TiO$_2$@RGO nanocomposite	Non-uniform deposition of Ce-TiO$_2$ with spherical crystalline TiO$_2$ on a reduced graphene oxide sheet.	quinalphos	Visible	-	20 mg/L	240	-	92	[352]
Ce-TiO$_2$@RGO nanocomposite	Non-uniform deposition of Ce-TiO$_2$ with spherical crystalline TiO$_2$ on a reduced graphene oxide sheet.	imidacloprid	Visible	-	20 mg/L	240	-	85	[352]
Ag$_3$PO$_4$/TiO$_2$ NPs	Crystallized structure with cubed shape Ag$_3$PO$_4$ and anatase TiO$_2$	2,4-dichlorophenoxyacetic acid	Visible	10 mg/L	1 g/L	60	3	98.4	[353]
2D/2D TiO$_2$/MIL88(Fe) (TCS@MOF) nanocomposite	Stacked layer thin MIL-88(Fe) nanosheet with micro-sized TiO$_2$ nano-granular spherical shape.	monocrotophos	visible	20 mg/L	0.05 g/L	30	5	~98.79%	[354]
TiO$_2$ nanotubes	Nanotubes	Simazine	UV	1 mg/L	-	54	-	48	[355]
TiO$_2$ NPs	Agglomerated spherical shape.	Acetamiprid	UV	4.5 mg/L	2000 mg/L	240	-	100	[356]
TiO$_2$ NPs	-	Imidaclopride	UV	25 mg/L	200 mg/L	48	-	90	[357]
TiO$_2$ NPs	-	1,2-dichloroethane	UV	100–200 mg/L	100 mg/L	360	7	95	[358]
N-doped TiO$_2$ nanoparticles	Agglomerated small particles.	dichlorodiphenyltrichloroethane	UV	10,000 mg/L	1000	48	7	70	[359]
lanthanide-doped TiO$_2$ photocatalysts	Solely anatase.	metazachlor	UV	10 mg/L	1000 mg/L	300	-	85	[360]

6. Challenges and Outlook

Despite the exquisite properties and the versatile applications of metal oxide nanomaterials and their composites, there are still inadequacies that cannot be ignored as the prepared material should be cost-effective, eco-friendly, and non-toxic. Recently, the use of functionalized metal oxides as adsorbents for the removal of pesticides has been riddled with many challenges. One challenge is the secondary waste produced from the adsorption process, which has not yet been addressed for the use of these materials as recycled materials in industries. Therefore, further studies on the implementation of the recycled metal oxides in the industrial field should be considered. Additionally, most of the published research neglects the fact that the water bodies are contaminated with multi-contaminants. Therefore, investigations should be conducted to assess the efficiency of metal oxides in the presence of multi-pollutants and a real representative matrix. Although the synthesized metal oxides have wide application, much of the research published does not include assessment on the toxicity of the material itself. It is very important to address and examine the toxicity of these materials and their composites, and to employ metal oxides as adsorbents and photocatalytic materials in commercial applications for the treatment of real samples.

7. Conclusions

Metal oxide nanomaterials and their composites have received considerable attention in recent years owing to their wide applications and eminent properties. Their porous structure, thermal stability, low toxicity, easy recovery, and large surface area make them extensively efficient for remediation applications as adsorbents and photocatalytic materials. Many publications have been collected on the removal of organic pesticides such as algaecides, fungicides, herbicides, insecticides, etc., using metal oxide nanomaterials and their nanocomposites, including metal oxides/metal-organic frameworks, metal oxides/polymers, metal/metal oxides other hybridized composites.

From the research reviewed, it can clearly be concluded that the prominent adsorptive interaction between metal oxides and pesticides is chemisorption. This finding is further supported by the type of mechanism and the type of kinetics, as the pseudo-second-order kinetic equation is used to express the chemisorption interaction. Additionally, the π–π interaction, π-complex interaction, and coordination or covalent bond are all types of chemical bonds. The adsorptive removal of pesticides using metal oxides has gained prominence due to its simplicity, effectivity, insensitivity, and flexibility. It has one limitation, in that it produces secondary products which need further recycling, decomposing, and management to be utilized in industries. Accordingly, photocatalytic degradation has emerged alternatively, which results in the complete mineralization of the pollutant to intermediates and H_2O and CO_2. Assessment of material toxicity should be focused on more, along with the by-products of adsorption. To scale up the material on an industrial scale, the investigated materials should be tested in real representative matrices that resemble the contaminated water.

Author Contributions: H.H.S., E.F.H.A. and A.H.K. prepared the manuscript, performing the literature survey and data interpretation. A.H.K., S.R. and A.A.A. revised the manuscript. A.A.A. provided the resources and financial support. All authors have read and agreed to the published version of the manuscript.

Funding: This research received no external funding.

Institutional Review Board Statement: Not applicable.

Informed Consent Statement: Not applicable.

Data Availability Statement: Data are available but not put in the public domain.

Conflicts of Interest: The authors declare no conflict of interest.

Abbreviations

POPs	Persistent organic chemicals
OCs	Organochlorines
OPs	Organophosphates
NPs	Nanoparticles
MO	Metal oxides
IONPs	Iron oxide nanoparticles
RT	Room temperature
ZnONPs-IPPs	Zinc oxide nanoparticles impregnated Pea peels
MOM-Fe3O4	Iron oxide nanoparticles with Moringa oleifera Lam. seeds
ZnO-CP	Zinc oxide with cucumber peel.
CTAB-ZnO	Cetyltrimethylammonium bromide functionalized Zinc oxide
BMTF-IL-ZnO	1-Butyl-3-methylimidazolium tetrafluoroborate functionalized Zinc oxide.
Hr-MgO	Hierarchical magnesium oxide
DDT	Dichloro-diphenyl-trichloroethane
PSO	Pseudo Second Order
PFO	Pseudo First Order
L	Langmuir isotherm model.
F	Freundlich isotherm model.
S	Sips isotherm model.
T	Temkin isotherm model.
D-A	Dubinin–Astakhov isotherm model.
e-	Electrostatic interaction
h	Hydrophobic interaction
π–π	π–π interaction
π-CM	π-complex formation
H	Hydrogen bond interaction
C	Coordination or covalent bond

References

1. Adebusuyi, A.T.; Sojinu, S.O.; Aleshinloye, A.O. The prevalence of persistent organic pollutants (POPs) in West Africa—A review. *Environ. Chall.* **2022**, *7*, 100486. [CrossRef]
2. Ighalo, J.O.; Yap, P.-S.; Iwuozor, K.O.; Aniagor, C.O.; Liu, T.; Dulta, K.; Iwuchukwu, F.U.; Rangabhashiyam, S. Adsorption of persistent organic pollutants (POPs) from the aqueous environment by nano-adsorbents: A review. *Environ. Res.* **2022**, *212*, 113123. [CrossRef] [PubMed]
3. Rani, M.; Shanker, U.; Jassal, V. Recent strategies for removal and degradation of persistent & toxic organochlorine pesticides using nanoparticles: A review. *J. Environ. Manag.* **2017**, *190*, 208–222. [CrossRef]
4. Billet, L.S.; Belskis, A.; Hoverman, J.T. Temperature affects the toxicity of pesticides to cercariae of the trematode Echinostoma trivolvis. *Aquat. Toxicol.* **2022**, *245*, 106102. [CrossRef]
5. Rasheed, T.; Rizwan, K.; Bilal, M.; Sher, F.; Iqbal, H.M.N. Tailored functional materials as robust candidates to mitigate pesticides in aqueous matrices—A review. *Chemosphere* **2021**, *282*, 131056. [CrossRef]
6. Parra-Arroyo, L.; González-González, R.B.; Castillo-Zacarías, C.; Melchor Martínez, E.M.; Sosa-Hernández, J.E.; Bilal, M.; Iqbal, H.M.N.; Barceló, D.; Parra-Saldívar, R. Highly hazardous pesticides and related pollutants: Toxicological, regulatory, and analytical aspects. *Sci. Total Environ.* **2022**, *807*, 151879. [CrossRef]
7. Cosgrove, S.; Jefferson, B.; Jarvis, P. Application of activated carbon fabric for the removal of a recalcitrant pesticide from agricultural run-off. *Sci. Total Environ.* **2022**, *815*, 152626. [CrossRef]
8. Tyagi, H.; Chawla, H.; Bhandari, H.; Garg, S. Recent-enhancements in visible-light photocatalytic degradation of organochlorines pesticides: A review. *Mater. Today Proc.* **2022**, *49*, 3289–3305. [CrossRef]
9. Islam, M.A.; Amin, S.M.N.; Rahman, M.A.; Juraimi, A.S.; Uddin, M.K.; Brown, C.L.; Arshad, A. Chronic effects of organic pesticides on the aquatic environment and human health: A review. *Environ. Nanotechnol. Monit. Manag.* **2022**, *18*, 100740. [CrossRef]
10. Wang, W.; Wang, X.; Cheng, N.; Luo, Y.; Lin, Y.; Xu, W.; Du, D. Recent advances in nanomaterials-based electrochemical (bio)sensors for pesticides detection. *TrAC Trends Anal. Chem.* **2020**, *132*, 116041. [CrossRef]
11. Wang, Y.; Wang, S.-L.; Xie, T.; Cao, J. Activated carbon derived from waste tangerine seed for the high-performance adsorption of carbamate pesticides from water and plant. *Bioresour. Technol.* **2020**, *316*, 123929. [CrossRef]

12. Boruah, P.K.; Darabdhara, G.; Das, M.R. Polydopamine functionalized graphene sheets decorated with magnetic metal oxide nanoparticles as efficient nanozyme for the detection and degradation of harmful triazine pesticides. *Chemosphere* **2021**, *268*, 129328. [CrossRef]

13. Bano, K.; Kaushal, S.; Singh, P.P. A review on photocatalytic degradation of hazardous pesticides using heterojunctions. *Polyhedron* **2021**, *209*, 115465. [CrossRef]

14. Huang, H.; Xia, C.; Liang, D.; Xie, Y.; Kong, F.; Fu, J.; Dou, Z.; Yang, Q.; Suo, W.; Zhang, Q.; et al. Removal and magnetic recovery of heavy metals and pesticides from soil by layered double hydroxides modified biotite. *Chem. Eng. J.* **2022**, *431*, 134113. [CrossRef]

15. Yeganeh, M.; Charkhloo, E.; Sobhi, H.R.; Esrafili, A.; Gholami, M. Photocatalytic processes associated with degradation of pesticides in aqueous solutions: Systematic review and meta-analysis. *Chem. Eng. J.* **2022**, *428*, 130081. [CrossRef]

16. Koe, W.S.; Lee, J.W.; Chong, W.C.; Pang, Y.L.; Sim, L.C. An overview of photocatalytic degradation: Photocatalysts, mechanisms, and development of photocatalytic membrane. *Environ. Sci. Pollut. Res.* **2020**, *27*, 2522–2565. [CrossRef]

17. Ni, J.; Lei, J.; Wang, Z.; Huang, L.; Zhu, H.; Liu, H.; Hu, F.; Qu, T.; Yang, H.; Yang, H.; et al. The Ultrahigh Adsorption Capacity and Excellent Photocatalytic Degradation Activity of Mesoporous CuO with Novel Architecture. *Nanomaterials* **2023**, *13*, 142. [CrossRef]

18. Dhananjay, B.; Pangarkar, V.; Beenackers, A. Photocatalytic Degradation for Environmental Application-A Review. *J. Chem. Technol. Biotechnol.* **2001**, *77*, 102–116. [CrossRef]

19. Jamshaid, M.; Nazir, M.A.; Najam, T.; Shah, S.S.A.; Khan, H.M.; Rehman, A.u. Facile synthesis of Yb^{3+}-Zn^{2+} substituted M type hexaferrites: Structural, electric and photocatalytic properties under visible light for methylene blue removal. *Chem. Phys. Lett.* **2022**, *805*, 139939. [CrossRef]

20. Ahmadi, A.; Hajilou, M.; Zavari, S.; Yaghmaei, S. A comparative review on adsorption and photocatalytic degradation of classified dyes with metal/non-metal-based modification of graphitic carbon nitride nanocomposites: Synthesis, mechanism, and affecting parameters. *J. Clean. Prod.* **2023**, *382*, 134967. [CrossRef]

21. Qumar, U.; Hassan, J.Z.; Bhatti, R.A.; Raza, A.; Nazir, G.; Nabgan, W.; Ikram, M. Photocatalysis vs adsorption by metal oxide nanoparticles. *J. Mater. Sci. Technol.* **2022**, *131*, 122–166. [CrossRef]

22. Gusain, R.; Gupta, K.; Joshi, P.; Khatri, O.P. Adsorptive removal and photocatalytic degradation of organic pollutants using metal oxides and their composites: A comprehensive review. *Adv. Colloid Interface Sci.* **2019**, *272*, 102009. [CrossRef] [PubMed]

23. Hua, M.; Zhang, S.; Pan, B.; Zhang, W.; Lv, L.; Zhang, Q. Heavy metal removal from water/wastewater by nanosized metal oxides: A review. *J. Hazard. Mater.* **2012**, *211–212*, 317–331. [CrossRef] [PubMed]

24. Farooq, U.; Ahmad, T.; Naaz, F.; Islam, S.u. Review on Metals and Metal Oxides in Sustainable Energy Production: Progress and Perspectives. *Energy Fuels* **2023**, *37*, 1577–1632. [CrossRef]

25. Selmani, A.; Kovačević, D.; Bohinc, K. Nanoparticles: From synthesis to applications and beyond. *Adv. Colloid Interface Sci.* **2022**, *303*, 102640. [CrossRef] [PubMed]

26. Bibi, S.; Ahmad, A.; Anjum, M.A.R.; Haleem, A.; Siddiq, M.; Shah, S.S.; Kahtani, A.A. Photocatalytic degradation of malachite green and methylene blue over reduced graphene oxide (rGO) based metal oxides (rGO-Fe_3O_4/TiO_2) nanocomposite under UV-visible light irradiation. *J. Environ. Chem. Eng.* **2021**, *9*, 105580. [CrossRef]

27. Khandare, D.; Mukherjee, S. A Review of Metal oxide Nanomaterials for Fluoride decontamination from Water Environment. *Mater. Today Proc.* **2019**, *18*, 1146–1155. [CrossRef]

28. Farooq, U.; Naz, F.; Phul, R.; Pandit, N.A.; Jain, S.K.; Ahmad, T. Development of Heterostructured Ferroelectric SrZrO3/CdS Photocatalysts with Enhanced Surface Area and Photocatalytic Activity. *J. Nanosci. Nanotechnol.* **2020**, *20*, 3770–3779. [CrossRef]

29. Jamshaid, M.; Khan, M.I.; Fernandez, J.; Shanableh, A.; Hussain, T.; Rehman, A.u. Synthesis of Ti^{4+} doped Ca-$BiFO_3$ for the enhanced photodegradation of moxifloxacin. *New J. Chem.* **2022**, *46*, 19848–19856. [CrossRef]

30. Shi, R.; Zhang, Z.; Luo, F. N-doped graphene-based CuO/WO_3/Cu composite material with performances of catalytic decomposition 4-nitrophenol and photocatalytic degradation of organic dyes. *Inorg. Chem. Commun.* **2020**, *121*, 108246. [CrossRef]

31. Wolski, L.; Grzelak, K.; Muńko, M.; Frankowski, M.; Grzyb, T.; Nowaczyk, G. Insight into photocatalytic degradation of ciprofloxacin over CeO_2/ZnO nanocomposites: Unravelling the synergy between the metal oxides and analysis of reaction pathways. *Appl. Surf. Sci.* **2021**, *563*, 150338. [CrossRef]

32. Wanjeri, V.W.O.; Sheppard, C.J.; Prinsloo, A.R.E.; Ngila, J.C.; Ndungu, P.G. Isotherm and kinetic investigations on the adsorption of organophosphorus pesticides on graphene oxide based silica coated magnetic nanoparticles functionalized with 2-phenylethylamine. *J. Environ. Chem. Eng.* **2018**, *6*, 1333–1346. [CrossRef]

33. Singh, A.; Sikarwar, S.; Verma, A.; Chandra Yadav, B. The recent development of metal oxide heterostructures based gas sensor, their future opportunities and challenges: A review. *Sens. Actuators A Phys.* **2021**, *332*, 113127. [CrossRef]

34. Wang, X.-L.; Sun, Y.-Y.; Xiao, Y.; Chen, X.-X.; Huang, X.-C.; Zhou, H.-L. Facile Solution-Refluxing Synthesis and Photocatalytic Dye Degradation of a Dynamic Covalent Organic Framework. *Molecules* **2022**, *27*, 8002. [CrossRef]

35. Nekooie, R.; Shamspur, T.; Mostafavi, A. Novel CuO/TiO_2/PANI nanocomposite: Preparation and photocatalytic investigation for chlorpyrifos degradation in water under visible light irradiation. *J. Photochem. Photobiol. A Chem.* **2021**, *407*, 113038. [CrossRef]

36. Shirzad-Siboni, M.; Jonidi-Jafari, A.; Farzadkia, M.; Esrafili, A.; Gholami, M. Enhancement of photocatalytic activity of Cu-doped ZnO nanorods for the degradation of an insecticide: Kinetics and reaction pathways. *J. Environ. Manag.* **2017**, *186*, 1–11. [CrossRef] [PubMed]

37. Hussain, I.; Lee, J.M.; Iqbal, S.; Kim, H.S.; Jang, S.W.; Jung, J.Y.; An, H.J.; Lamiel, C.; Mohamed, S.G.; Lee, Y.R.; et al. Preserved crystal phase and morphology: Electrochemical influence of copper and iron co-doped cobalt oxide and its supercapacitor applications. *Electrochim. Acta* **2020**, *340*, 135953. [CrossRef]
38. Gopinath, S.; Mayakannan, M.; Vetrivel, S. Structural, optical, morphological properties of silver doped cobalt oxide nanoparticles by microwave irradiation method. *Ceram. Int.* **2022**, *48*, 6103–6115. [CrossRef]
39. Rasheed, T.; Nabeel, F.; Bilal, M.; Iqbal, H.M.N. Biogenic synthesis and characterization of cobalt oxide nanoparticles for catalytic reduction of direct yellow-142 and methyl orange dyes. *Biocatal. Agric. Biotechnol.* **2019**, *19*, 101154. [CrossRef]
40. Letsholathebe, D.; Thema, F.T.; Mphale, K.; Mohamed, H.E.A.; Holonga, K.J.; Ketlhwaafetse, R.; Chimidza, S. Optical and structural stability of Co$_3$O$_4$ nanoparticles for photocatalytic applications. *Mater. Today Proc.* **2021**, *36*, 499–503. [CrossRef]
41. Dharaskar, S.; Kodgire, P.; Bansod, P. Enhanced diesel properties with energy efficient nano-aluminium oxide and nano-cobalt oxide particles. *Mater. Today Proc.* **2021**, *62*, 6927–6933. [CrossRef]
42. Dey, S.; Dhal, G.C. The catalytic activity of cobalt nanoparticles for low-temperature oxidation of carbon monoxide. *Mater. Today Chem.* **2019**, *14*, 100198. [CrossRef]
43. Uddin, M.K.; Baig, U. Synthesis of Co$_3$O$_4$ nanoparticles and their performance towards methyl orange dye removal: Characterisation, adsorption and response surface methodology. *J. Clean. Prod.* **2019**, *211*, 1141–1153. [CrossRef]
44. Lima, A.F. Interpretation of the optical absorption spectrum of Co$_3$O$_4$ with normal spinel structure from first principles calculations. *J. Phys. Chem. Solids* **2014**, *75*, 148–152. [CrossRef]
45. Asha, G.; Rajeshwari, V.; Stephen, G.; Gurusamy, S.; Carolin Jeniba Rachel, D. Eco-friendly synthesis and characterization of cobalt oxide nanoparticles by sativum species and its photo-catalytic activity. *Mater. Today Proc.* **2022**, *48*, 486–493. [CrossRef]
46. Navarrete, È.; Bittencourt, C.; Noirfalise, X.; Umek, P.; González, E.; Güell, F.; Llobet, E. WO$_3$ nanowires loaded with cobalt oxide nanoparticles, deposited by a two-step AACVD for gas sensing applications. *Sens. Actuators B Chem.* **2019**, *298*, 126868. [CrossRef]
47. Jincy, C.S.; Meena, P. Evaluation of cytotoxic activity of Fe doped cobalt oxide nanoparticles. *J. Trace Elem. Med. Biol.* **2022**, *70*, 126916. [CrossRef]
48. Gaikar, P.S.; Angre, A.P.; Wadhawa, G.; Ledade, P.V.; Mahmood, S.H.; Lambat, T.L. Green synthesis of cobalt oxide thin films as an electrode material for electrochemical capacitor application. *Curr. Res. Green Sustain. Chem.* **2022**, *5*, 100265. [CrossRef]
49. Lakra, R.; Kumar, R.; Sahoo, P.K.; Sharma, D.; Thatoi, D.; Soam, A. Facile synthesis of cobalt oxide and graphene nanosheets nanocomposite for aqueous supercapacitor application. *Carbon Trends* **2022**, *7*, 100144. [CrossRef]
50. Rakotonarivo, E.F.; Abouloula, C.N.; Narjis, A.; Nkhaili, L.; Brouillette, F.; Oueriagli, A. Optimization of the electrodeposition of the pure and cobalt doped copper oxide for solar cells and other applications. *Phys. B Condens. Matter* **2021**, *609*, 412783. [CrossRef]
51. Jincy, C.S.; Meena, P. Synthesis, characterization, and NH3 gas sensing application of Zn doped cobalt oxide nanoparticles. *Inorg. Chem. Commun.* **2020**, *120*, 108145. [CrossRef]
52. Ni, Q.; Ma, J.; Fan, C.; Kong, Y.; Peng, M.; Komarneni, S. Spinel-type cobalt-manganese oxide catalyst for degradation of Orange II using a novel heterogeneous photo-chemical catalysis system. *Ceram. Int.* **2018**, *44*, 19474–19480. [CrossRef]
53. Feng, H.; Liang, L.; Ge, J.; Wu, W.; Huang, Z.; Liu, Y.; Li, L. Delicate manipulation of cobalt oxide nanodot clusterization on binder-free TiO$_2$-nanorod photoanodes for efficient photoelectrochemical catalysis. *J. Alloys Compd.* **2020**, *820*, 153139. [CrossRef]
54. Ullah, R.; Rasheed, M.A.; Abbas, S.; Rehman, K.-u.; Shah, A.; Ullah, K.; Khan, Y.; Bibi, M.; Ahmad, M.; Ali, G. Electrochemical sensing of H2O2 using cobalt oxide modified TiO$_2$ nanotubes. *Curr. Appl. Phys.* **2022**, *38*, 40–48. [CrossRef]
55. Wang, F.; Li, H.; Yuan, Z.; Sun, Y.; Chang, F.; Deng, H.; Xie, L.; Li, H. A highly sensitive gas sensor based on CuO nanoparticles synthetized via a sol–gel method. *RSC Adv.* **2016**, *6*, 79343–79349. [CrossRef]
56. Censabella, M.; Iacono, V.; Scandurra, A.; Moulaee, K.; Neri, G.; Ruffino, F.; Mirabella, S. Low temperature detection of nitric oxide by CuO nanoparticles synthesized by pulsed laser ablation. *Sens. Actuators B Chem.* **2022**, *358*, 131489. [CrossRef]
57. Heinemann, M.; Eifert, B.; Heiliger, C. Band structure and phase stability of the copper oxides Cu$_2$O, CuO, and Cu$_4$O$_3$. *Phys. Rev. B* **2013**, *87*, 115111. [CrossRef]
58. Wojcieszak, D.; Obstarczyk, A.; Mańkowska, E.; Mazur, M.; Kaczmarek, D.; Zakrzewska, K.; Mazur, P.; Domaradzki, J. Thermal oxidation impact on the optoelectronic and hydrogen sensing properties of p-type copper oxide thin films. *Mater. Res. Bull.* **2022**, *147*, 111646. [CrossRef]
59. Kim, H.; Park, S.; Park, Y.; Choi, D.; Yoo, B.; Lee, C.S. Fabrication of a semi-transparent flexible humidity sensor using kinetically sprayed cupric oxide film. *Sens. Actuators B Chem.* **2018**, *274*, 331–337. [CrossRef]
60. Moghanlou, A.O.; Sadr, M.H.; Bezaatpour, A.; Salimi, F.; Yosefi, M. RGO/Cu$_2$O-CuO nanocomposite as a visible-light assisted photocatalyst for reduction of organic nitro groups to amines. *Mol. Catal.* **2021**, *516*, 111997. [CrossRef]
61. Vázquez-Vargas, D.A.; Amézaga-Madrid, P.; Jáuregui-Martínez, L.E.; Esquivel-Pereyra, O.; Antúnez-Flores, W.; Pizá-Ruiz, P.; Miki-Yoshida, M. Synthesis and microstructural characterization of cupric oxide and cobalt oxide nanostructures for their application as selective solar coatings. *Thin Solid Film.* **2020**, *706*, 138046. [CrossRef]
62. Maruthupandy, M.; Zuo, Y.; Chen, J.-S.; Song, J.-M.; Niu, H.-L.; Mao, C.-J.; Zhang, S.-Y.; Shen, Y.-H. Synthesis of metal oxide nanoparticles (CuO and ZnO NPs) via biological template and their optical sensor applications. *Appl. Surf. Sci.* **2017**, *397*, 167–174. [CrossRef]
63. Mohammed Ali, M.J.; Radhy, M.M.; mashkoor, S.J.; Ali, E.M. Synthesis and characterization of copper oxide nanoparticles and their application for solar cell. *Mater. Today Proc.* **2021**, *60*, 917–921. [CrossRef]

64. Pourbeyram, S.; Abdollahpour, J.; Soltanpour, M. Green synthesis of copper oxide nanoparticles decorated reduced graphene oxide for high sensitive detection of glucose. *Mater. Sci. Eng. C* **2019**, *94*, 850–857. [CrossRef]

65. Nabila, M.I.; Kannabiran, K. Biosynthesis, characterization and antibacterial activity of copper oxide nanoparticles (CuO NPs) from actinomycetes. *Biocatal. Agric. Biotechnol.* **2018**, *15*, 56–62. [CrossRef]

66. Kim, T.K.; VanSaders, B.; Moon, J.; Kim, T.; Liu, C.-H.; Khamwannah, J.; Chun, D.; Choi, D.; Kargar, A.; Chen, R.; et al. Tandem structured spectrally selective coating layer of copper oxide nanowires combined with cobalt oxide nanoparticles. *Nano Energy* **2015**, *11*, 247–259. [CrossRef]

67. Nwanya, A.C.; Razanamahandry, L.C.; Bashir, A.K.H.; Ikpo, C.O.; Nwanya, S.C.; Botha, S.; Ntwampe, S.K.O.; Ezema, F.I.; Iwuoha, E.I.; Maaza, M. Industrial textile effluent treatment and antibacterial effectiveness of *Zea mays* L. Dry husk mediated bio-synthesized copper oxide nanoparticles. *J. Hazard. Mater.* **2019**, *375*, 281–289. [CrossRef]

68. McDonald, K.J.; Reynolds, B.; Reddy, K.J. Intrinsic properties of cupric oxide nanoparticles enable effective filtration of arsenic from water. *Sci. Rep.* **2015**, *5*, 11110. [CrossRef]

69. Srivastava, V.; Choubey, A.K. Investigation of adsorption of organic dyes present in wastewater using chitosan beads immobilized with biofabricated CuO nanoparticles. *J. Mol. Struct.* **2021**, *1242*, 130749. [CrossRef]

70. Naaz, F.; Sharma, A.; Shahazad, M.; Ahmad, T. Hydrothermally Derived Hierarchical CuO Nanoflowers as an Efficient Photocatalyst and Electrocatalyst for Hydrogen Evolution. *ChemistrySelect* **2022**, *7*, e202201800. [CrossRef]

71. Gupta, K.; Chundawat, T.S. Zinc oxide nanoparticles synthesized using Fusarium oxysporum to enhance bioethanol production from rice-straw. *Biomass Bioenergy* **2020**, *143*, 105840. [CrossRef]

72. Bandeira, M.; Possan, A.L.; Pavin, S.S.; Raota, C.S.; Vebber, M.C.; Giovanela, M.; Roesch-Ely, M.; Devine, D.M.; Crespo, J.S. Mechanism of formation, characterization and cytotoxicity of green synthesized zinc oxide nanoparticles obtained from Ilex paraguariensis leaves extract. *Nano-Struct. Nano-Objects* **2020**, *24*, 100532. [CrossRef]

73. Darvishi, E.; Kahrizi, D.; Arkan, E. Comparison of different properties of zinc oxide nanoparticles synthesized by the green (using *Juglans regia* L. leaf extract) and chemical methods. *J. Mol. Liq.* **2019**, *286*, 110831. [CrossRef]

74. Sultana, K.A.; Islam, M.T.; Silva, J.A.; Turley, R.S.; Hernandez-Viezcas, J.A.; Gardea-Torresdey, J.L.; Noveron, J.C. Sustainable synthesis of zinc oxide nanoparticles for photocatalytic degradation of organic pollutant and generation of hydroxyl radical. *J. Mol. Liq.* **2020**, *307*, 112931. [CrossRef]

75. Dkhil, M.A.; Diab, M.S.M.; Aljawdah, H.M.A.; Murshed, M.; Hafiz, T.A.; Al-Quraishy, S.; Bauomy, A.A. Neuro-biochemical changes induced by zinc oxide nanoparticles. *Saudi J. Biol. Sci.* **2020**, *27*, 2863–2867. [CrossRef] [PubMed]

76. Brindhadevi, K.; Samuel, M.S.; Verma, T.N.; Vasantharaj, S.; Sathiyavimal, S.; Saravanan, M.; Pugazhendhi, A.; Duc, P.A. Zinc oxide nanoparticles (ZnONPs) -induced antioxidants and photocatalytic degradation activity from hybrid grape pulp extract (HGPE). *Biocatal. Agric. Biotechnol.* **2020**, *28*, 101730. [CrossRef]

77. Dang, Z.; Sun, J.; Fan, J.; Li, J.; Li, X.; Chen, T. Zinc oxide spiky nanoparticles: A promising nanomaterial for killing tumor cells. *Mater. Sci. Eng. C* **2021**, *124*, 112071. [CrossRef]

78. Shankar, S.; Rhim, J.-W. Effect of types of zinc oxide nanoparticles on structural, mechanical and antibacterial properties of poly(lactide)/poly(butylene adipate-co-terephthalate) composite films. *Food Packag. Shelf Life* **2019**, *21*, 100327. [CrossRef]

79. Jayachandran, A.; Aswathy, T.R.; Nair, A.S. Green synthesis and characterization of zinc oxide nanoparticles using *Cayratia pedata* leaf extract. *Biochem. Biophys. Rep.* **2021**, *26*, 100995. [CrossRef]

80. Bandeira, M.; Giovanela, M.; Roesch-Ely, M.; Devine, D.M.; da Silva Crespo, J. Green synthesis of zinc oxide nanoparticles: A review of the synthesis methodology and mechanism of formation. *Sustain. Chem. Pharm.* **2020**, *15*, 100223. [CrossRef]

81. Ranjithkumar, B.; Ramalingam, H.B.; Kumar, E.R.; Srinivas, C.; Magesh, G.; Rahale, C.S.; El-Metwaly, N.M.; Shekar, B.C. Natural fuels (Honey and Cow urine) assisted combustion synthesis of zinc oxide nanoparticles for antimicrobial activities. *Ceram. Int.* **2021**, *47*, 14475–14481. [CrossRef]

82. Archana, P.; Janarthanan, B.; Bhuvana, S.; Rajiv, P.; Sharmila, S. Concert of zinc oxide nanoparticles synthesized using *Cucumis melo* by green synthesis and the antibacterial activity on pathogenic bacteria. *Inorg. Chem. Commun.* **2022**, *137*, 109255. [CrossRef]

83. Espitia, P.J.P.; Soares, N.d.F.F.; Coimbra, J.S.d.R.; de Andrade, N.J.; Cruz, R.S.; Medeiros, E.A.A. Zinc Oxide Nanoparticles: Synthesis, Antimicrobial Activity and Food Packaging Applications. *Food Bioprocess Technol.* **2012**, *5*, 1447–1464. [CrossRef]

84. Rajbongshi, B.M.; Samdarshi, S.K. Cobalt-doped zincblende–wurtzite mixed-phase ZnO photocatalyst nanoparticles with high activity in visible spectrum. *Appl. Catal. B Environ.* **2014**, *144*, 435–441. [CrossRef]

85. Doan Thi, T.U.; Nguyen, T.T.; Thi, Y.D.; Ta Thi, K.H.; Phan, B.T.; Pham, K.N. Green synthesis of ZnO nanoparticles using orange fruit peel extract for antibacterial activities. *RSC Adv.* **2020**, *10*, 23899–23907. [CrossRef]

86. Kanimozhi, S.; Prabu, K.M.; Thambidurai, S.; Suresh, S. Dye-sensitized solar cell performance and photocatalytic activity enhancement using binary zinc oxide-copper oxide nanocomposites prepared via co-precipitation route. *Ceram. Int.* **2021**, *47*, 30234–30246. [CrossRef]

87. Rakha, A.A.; Shahzad, M.; Ghaffar, A.; Javed, K.; Pervez, A.; Sarwar, N.; Munam, M. Power conversion efficiency of hybrid solar cells based on Camellia sinensis doped polyvinyl alcohol and ZnO nanoparticles. *Opt. Mater.* **2021**, *120*, 111434. [CrossRef]

88. Abood, M.K.; Fayad, M.A.; Al Salihi, H.A.; Salbi, H.A.A. Effect of ZnO nanoparticles deposition on porous silicon solar cell. *Mater. Today Proc.* **2021**, *42*, 2935–2940. [CrossRef]

89. Hanabaratti, R.M.; Tuwar, S.M.; Nandibewoor, S.T.; Gowda, J.I. Fabrication and characterization of zinc oxide nanoparticles modified glassy carbon electrode for sensitive determination of paracetamol. *Chem. Data Collect.* **2020**, *30*, 100540. [CrossRef]

90. Hussein, H.T.; Kareem, M.H.; Abdul Hussein, A.M. Synthesis and characterization of carbon nanotube doped with zinc oxide nanoparticles CNTs-ZnO/PS as ethanol gas sensor. *Optik* **2021**, *248*, 168107. [CrossRef]

91. Chelladurai, M.; Margavelu, G.; Vijayakumar, S.; González-Sánchez, Z.I.; Vijayan, K.; Sahadevan, R. Preparation and characterization of amine-functionalized mupirocin-loaded zinc oxide nanoparticles: A potent drug delivery agent in targeting human epidermoid carcinoma (A431) cells. *J. Drug Deliv. Sci. Technol.* **2022**, *70*, 103244. [CrossRef]

92. Singh, T.A.; Das, J.; Sil, P.C. Zinc oxide nanoparticles: A comprehensive review on its synthesis, anticancer and drug delivery applications as well as health risks. *Adv. Colloid Interface Sci.* **2020**, *286*, 102317. [CrossRef]

93. Paiva-Santos, A.C.; Herdade, A.M.; Guerra, C.; Peixoto, D.; Pereira-Silva, M.; Zeinali, M.; Mascarenhas-Melo, F.; Paranhos, A.; Veiga, F. Plant-mediated green synthesis of metal-based nanoparticles for dermopharmaceutical and cosmetic applications. *Int. J. Pharm.* **2021**, *597*, 120311. [CrossRef] [PubMed]

94. Mustapha, S.; Ndamitso, M.M.; Abdulkareem, A.S.; Tijani, J.O.; Shuaib, D.T.; Ajala, A.O.; Mohammed, A.K. Application of TiO$_2$ and ZnO nanoparticles immobilized on clay in wastewater treatment: A review. *Appl. Water Sci.* **2020**, *10*, 49. [CrossRef]

95. Aksu Demirezen, D.; Yıldız, Y.Ş.; Yılmaz, Ş.; Demirezen Yılmaz, D. Green synthesis and characterization of iron oxide nanoparticles using Ficus carica (common fig) dried fruit extract. *J. Biosci. Bioeng.* **2019**, *127*, 241–245. [CrossRef]

96. Yu, X.; Zhou, J. Grain boundary in oxide scale during high-temperature metal processing. *Study Grain Bound. Character* **2017**, 59–77. [CrossRef]

97. Machala, L.; Tuček, J.; Zbořil, R. Polymorphous Transformations of Nanometric Iron(III) Oxide: A Review. *Chem. Mater.* **2011**, *23*, 3255–3272. [CrossRef]

98. Lassoued, A.; Lassoued, M.S.; Dkhil, B.; Ammar, S.; Gadri, A. Synthesis, structural, morphological, optical and magnetic characterization of iron oxide (α-Fe$_2$O$_3$) nanoparticles by precipitation method: Effect of varying the nature of precursor. *Phys. E Low-Dimens. Syst. Nanostruct.* **2018**, *97*, 328–334. [CrossRef]

99. Ong, H.T.; Suppiah, D.D.; Muhd Julkapli, N. Fatty acid coated iron oxide nanoparticle: Effect on stability, particle size and magnetic properties. *Colloids Surf. A Physicochem. Eng. Asp.* **2020**, *606*, 125371. [CrossRef]

100. Borges, R.; Mendonça-Ferreira, L.; Rettori, C.; Pereira, I.S.O.; Baino, F.; Marchi, J. New sol-gel-derived magnetic bioactive glass-ceramics containing superparamagnetic hematite nanocrystals for hyperthermia application. *Mater. Sci. Eng. C* **2021**, *120*, 111692. [CrossRef]

101. Karaagac, O.; Köçkar, H. Improvement of the saturation magnetization of PEG coated superparamagnetic iron oxide nanoparticles. *J. Magn. Magn. Mater.* **2022**, *551*, 169140. [CrossRef]

102. Al-Jabari, M.H.; Sulaiman, S.; Ali, S.; Barakat, R.; Mubarak, A.; Khan, S.A. Adsorption study of levofloxacin on reusable magnetic nanoparticles: Kinetics and antibacterial activity. *J. Mol. Liq.* **2019**, *291*, 111249. [CrossRef]

103. Shi, S.-F.; Jia, J.-F.; Guo, X.-K.; Zhao, Y.-P.; Chen, D.-S.; Guo, Y.-Y.; Cheng, T.; Zhang, X.-L. Biocompatibility of chitosan-coated iron oxide nanoparticles with osteoblast cells. *Int. J. Nanomed.* **2012**, *7*, 5593.

104. Unsoy, G.; Yalcin, S.; Khodadust, R.; Gündüz, G.; Gunduz, U. Synthesis optimization and characterization of chitosan-coated iron oxide nanoparticles produced for biomedical applications. *J. Nanopart. Res.* **2012**, *14*, 964. [CrossRef]

105. Lopez, J.D.; Keley, M.; Dante, A.; Werneck, M.M. Optical fiber sensor coated with copper and iron oxide nanoparticles for hydrogen sulfide sensing. *Opt. Fiber Technol.* **2021**, *67*, 102731. [CrossRef]

106. Pakapongpan, S.; Poo-arporn, Y.; Tuantranont, A.; Poo-arporn, R.P. A facile one-pot synthesis of magnetic iron oxide nanoparticles embed N-doped graphene modified magnetic screen printed electrode for electrochemical sensing of chloramphenicol and diethylstilbestrol. *Talanta* **2022**, *241*, 123184. [CrossRef] [PubMed]

107. Tung, T.T.; Chien, N.V.; Van Duy, N.; Van Hieu, N.; Nine, M.J.; Coghlan, C.J.; Tran, D.N.H.; Losic, D. Magnetic iron oxide nanoparticles decorated graphene for chemoresistive gas sensing: The particle size effects. *J. Colloid Interface Sci.* **2019**, *539*, 315–325. [CrossRef]

108. Roy, S.D.; Das, K.C.; Dhar, S.S. Conventional to green synthesis of magnetic iron oxide nanoparticles; its application as catalyst, photocatalyst and toxicity: A short review. *Inorg. Chem. Commun.* **2021**, *134*, 109050. [CrossRef]

109. Moodley, P.; Scheijen, F.J.E.; Niemantsverdriet, J.W.; Thüne, P.C. Iron oxide nanoparticles on flat oxidic surfaces—Introducing a new model catalyst for Fischer–Tropsch catalysis. *Catal. Today* **2010**, *154*, 142–148. [CrossRef]

110. Carrillo, A.I.; Serrano, E.; Luque, R.; García-Martínez, J. Microwave-assisted catalysis by iron oxide nanoparticles on MCM-41: Effect of the support morphology. *Appl. Catal. A Gen.* **2013**, *453*, 383–390. [CrossRef]

111. Fatimah, I.; Amaliah, S.N.; Andrian, M.F.; Handayani, T.P.; Nurillahi, R.; Prakoso, N.I.; Wicaksono, W.P.; Chuenchom, L. Iron oxide nanoparticles supported on biogenic silica derived from bamboo leaf ash for rhodamine B photodegradation. *Sustain. Chem. Pharm.* **2019**, *13*, 100149. [CrossRef]

112. Algarín, M.; Amaya, M.; Solano, R.; Patiño-Ruiz, D.; Herrera, A. Synthesis of a magnetic iron oxide/zinc oxide engineered nanocatalyst for enhanced visible-light photodegradation of Cartasol brilliant violet 5BFN in aqueous solution. *Nano-Struct. Nano-Objects* **2021**, *26*, 100730. [CrossRef]

113. Alves, F.H.d.O.; Araújo, O.A.; de Oliveira, A.C.; Garg, V.K. Preparation and characterization of PAni(CA)/Magnetic iron oxide hybrids and evaluation in adsorption/photodegradation of blue methylene dye. *Surf. Interfaces* **2021**, *23*, 100954. [CrossRef]

114. Xu, H.; Yuan, H.; Yu, J.; Lin, S. Study on the competitive adsorption and correlational mechanism for heavy metal ions using the carboxylated magnetic iron oxide nanoparticles (MNPs-COOH) as efficient adsorbents. *Appl. Surf. Sci.* **2019**, *473*, 960–966. [CrossRef]

115. Lin, S.; Liu, L.; Yang, Y.; Lin, K. Study on preferential adsorption of cationic-style heavy metals using amine-functionalized magnetic iron oxide nanoparticles (MIONPs-NH2) as efficient adsorbents. *Appl. Surf. Sci.* **2017**, *407*, 29–35. [CrossRef]

116. Javid, A.; Ahmadian, S.; Saboury, A.; Kalantar, M.; Rezaei-Zarchi, S. Chitosan-Coated Superparamagnetic Iron Oxide Nanoparticles for Doxorubicin Delivery: Synthesis and Anticancer Effect Against Human Ovarian Cancer Cells. *Chem. Biol. Drug Des.* **2013**, *82*, 296–306. [CrossRef]

117. Jain, M.; Yadav, M.; Kohout, T.; Lahtinen, M.; Garg, V.K.; Sillanpää, M. Development of iron oxide/activated carbon nanoparticle composite for the removal of Cr(VI), Cu(II) and Cd(II) ions from aqueous solution. *Water Resour. Ind.* **2018**, *20*, 54–74. [CrossRef]

118. Wei, Y.; Zhu, J.; Gan, Y.; Cheng, G. Titanium glycolate-derived TiO_2 nanomaterials: Synthesis and applications. *Adv. Powder Technol.* **2018**, *29*, 2289–2311. [CrossRef]

119. Bortamuly, R.; Naresh, V.; Das, M.R.; Kumar, V.K.; Muduli, S.; Martha, S.K.; Saikia, P. Titania supported bio-derived activated carbon as an electrode material for high-performance supercapacitors. *J. Energy Storage* **2021**, *42*, 103144. [CrossRef]

120. Zhang, Y.; Yang, H.M.; Park, S.-J. Synthesis and characterization of nitrogen-doped TiO_2 coatings on reduced graphene oxide for enhancing the visible light photocatalytic activity. *Curr. Appl. Phys.* **2018**, *18*, 163–169. [CrossRef]

121. Pérez-Jiménez, L.E.; Solis-Cortazar, J.C.; Rojas-Blanco, L.; Perez-Hernandez, G.; Martinez, O.S.; Palomera, R.C.; Paraguay-Delgado, F.; Zamudio-Torres, I.; Morales, E.R. Enhancement of optoelectronic properties of TiO_2 films containing Pt nanoparticles. *Results Phys.* **2019**, *12*, 1680–1685. [CrossRef]

122. Bayan, E.M.; Lupeiko, T.G.; Pustovaya, L.E.; Volkova, M.G.; Butova, V.V.; Guda, A.A. Zn–F co-doped TiO_2 nanomaterials: Synthesis, structure and photocatalytic activity. *J. Alloys Compd.* **2020**, *822*, 153662. [CrossRef]

123. Haggerty, J.E.; Schelhas, L.T.; Kitchaev, D.A.; Mangum, J.S.; Garten, L.M.; Sun, W.; Stone, K.H.; Perkins, J.D.; Toney, M.F.; Ceder, G. High-fraction brookite films from amorphous precursors. *Sci. Rep.* **2017**, *7*, 15232. [CrossRef] [PubMed]

124. Zhang, J.; Yan, S.; Fu, L.; Wang, F.; Yuan, M.; Luo, G.; Xu, Q.; Wang, X.; Li, C. Photocatalytic Degradation of Rhodamine B on Anatase, Rutile, and Brookite TiO_2. *Chin. J. Catal.* **2011**, *32*, 983–991. [CrossRef]

125. Kumar, S.G.; Rao, K.S.R.K. Comparison of modification strategies towards enhanced charge carrier separation and photocatalytic degradation activity of metal oxide semiconductors (TiO_2, WO_3 and ZnO). *Appl. Surf. Sci.* **2017**, *391*, 124–148. [CrossRef]

126. Harlapur, S.F.; Rashmi, B.N.; Nagaswarupa, H.P.; Prashantha, S.C.; Shashishekar, T.R.; Anil Kumar, M.R. Photocatalytic studies of TiO_2 nanomaterials prepared via facile wet chemical route. *Mater. Today Proc.* **2017**, *4*, 11713–11719. [CrossRef]

127. Umar, A.A.; Rahman, M.Y.A.; Saad, S.K.M.; Salleh, M.M.; Oyama, M. Preparation of grass-like TiO_2 nanostructure thin films: Effect of growth temperature. *Appl. Surf. Sci.* **2013**, *270*, 109–114. [CrossRef]

128. D'Arienzo, M.; Scotti, R.; Di Credico, B.; Redaelli, M. Chapter 13—Synthesis and Characterization of Morphology-Controlled TiO_2 Nanocrystals: Opportunities and Challenges for their Application in Photocatalytic Materials. In *Studies in Surface Science and Catalysis*; Fornasiero, P., Cargnello, M., Eds.; Elsevier: Amsterdam, The Netherlands, 2017; Volume 177, pp. 477–540.

129. Fan, Z.; Meng, F.; Zhang, M.; Wu, Z.; Sun, Z.; Li, A. Solvothermal synthesis of hierarchical TiO_2 nanostructures with tunable morphology and enhanced photocatalytic activity. *Appl. Surf. Sci.* **2016**, *360*, 298–305. [CrossRef]

130. Narzary, S.; Alamelu, K.; Raja, V.; Jaffar Ali, B.M. Visible light active, magnetically retrievable Fe3O4@SiO2@g-C3N4/TiO2 nanocomposite as efficient photocatalyst for removal of dye pollutants. *J. Environ. Chem. Eng.* **2020**, *8*, 104373. [CrossRef]

131. Qiao, H.; Xiao, H.; Huang, Y.; Yuan, C.; Zhang, X.; Bu, X.; Wang, Z.; Han, S.; Zhang, L.; Su, Z.; et al. SiO2 loading into polydopamine-functionalized TiO2 nanotubes for biomedical applications. *Surf. Coat. Technol.* **2019**, *364*, 170–179. [CrossRef]

132. Malevu, T.D. Ball Milling synthesis and characterization of highly crystalline TiO_2-ZnO hybrids for photovoltaic applications. *Phys. B Condens. Matter* **2021**, *621*, 413291. [CrossRef]

133. Ullah, F.; Qureshi, M.T.; Sultana, K.; Saleem, M.; Al Elaimi, M.; Abdel Hameed, R.; Haq, S.u.; Ismail, H.S.; Anwar, M.S. Structural and dielectric studies of $MgAl_2O_4$–TiO_2 composites for energy storage applications. *Ceram. Int.* **2021**, *47*, 30665–30670. [CrossRef]

134. Abinaya, S.; Kavitha, H.P.; Prakash, M.; Muthukrishnaraj, A. Green synthesis of magnesium oxide nanoparticles and its applications: A review. *Sustain. Chem. Pharm.* **2021**, *19*, 100368. [CrossRef]

135. Nagappa, B.; Chandrappa, G.T. Mesoporous nanocrystalline magnesium oxide for environmental remediation. *Microporous Mesoporous Mater.* **2007**, *106*, 212–218. [CrossRef]

136. Mehta, M.; Mukhopadhyay, M.; Christian, R.; Mistry, N. Synthesis and characterization of MgO nanocrystals using strong and weak bases. *Powder Technol.* **2012**, *226*, 213–221. [CrossRef]

137. Abdulkhaleq, N.A.; Nayef, U.M.; Albarazanchi, A.K.H. MgO nanoparticles synthesis via laser ablation stationed on porous silicon for photoconversion application. *Optik* **2020**, *212*, 164793. [CrossRef]

138. Saito, A.; Obata, S.; Nishina, Y. Uniform coating of magnesium oxide crystal with reduced graphene oxide achieves moisture barrier performance. *Appl. Surf. Sci.* **2022**, *573*, 151483. [CrossRef]

139. Sivaselvam, S.; Premasudha, P.; Viswanathan, C.; Ponpandian, N. Enhanced removal of emerging pharmaceutical contaminant ciprofloxacin and pathogen inactivation using morphologically tuned MgO nanostructures. *J. Environ. Chem. Eng.* **2020**, *8*, 104256. [CrossRef]

140. Alkhudhayri, A.; Thagfan, F.A.; Al-Quraishy, S.; Abdel-Gaber, R.; Dkhil, M.A. Assessment of the oxidative status and goblet cell response during eimeriosis and after treatment of mice with magnesium oxide nanoparticles. *Saudi J. Biol. Sci.* **2022**, *29*, 1234–1238. [CrossRef]

141. El-Sawy, N.M.; Raafat, A.I.; Badawy, N.A.; Mohamed, A.M. Radiation development of pH-responsive (xanthan-acrylic acid)/MgO nanocomposite hydrogels for controlled delivery of methotrexate anticancer drug. *Int. J. Biol. Macromol.* **2020**, *142*, 254–264. [CrossRef]

142. Zheng, X.; Feng, S.; Wang, X.; Shi, Z.; Mao, Y.; Zhao, Q.; Wang, S. MSNCs and MgO-MSNCs as drug delivery systems to control the adsorption kinetics and release rate of indometacin. *Asian J. Pharm. Sci.* **2019**, *14*, 275–286. [CrossRef]

143. Yang, S.; Liang, L.; Liu, L.; Yin, Y.; Liu, Y.; Lei, G.; Zhou, K.; Huang, Q.; Wu, H. Using MgO nanoparticles as a potential platform to precisely load and steadily release Ag ions for enhanced osteogenesis and bacterial killing. *Mater. Sci. Eng. C* **2021**, *119*, 111399. [CrossRef]

144. Nigam, A.; Saini, S.; Rai, A.K.; Pawar, S.J. Structural, optical, cytotoxicity, and antimicrobial properties of MgO, ZnO and MgO/ZnO nanocomposite for biomedical applications. *Ceram. Int.* **2021**, *47*, 19515–19525. [CrossRef]

145. Karthik, K.; Dhanuskodi, S.; Gobinath, C.; Prabukumar, S.; Sivaramakrishnan, S. Fabrication of MgO nanostructures and its efficient photocatalytic, antibacterial and anticancer performance. *J. Photochem. Photobiol. B Biol.* **2019**, *190*, 8–20. [CrossRef]

146. Nguyen, D.T.C.; Dang, H.H.; Vo, D.-V.N.; Bach, L.G.; Nguyen, T.D.; Tran, T.V. Biogenic synthesis of MgO nanoparticles from different extracts (flower, bark, leaf) of *Tecoma stans* (L.) and their utilization in selected organic dyes treatment. *J. Hazard. Mater.* **2021**, *404*, 124146. [CrossRef]

147. Štengl, V.; Bakardjieva, S.; Maříková, M.; Bezdička, P.; Šubrt, J. Magnesium oxide nanoparticles prepared by ultrasound enhanced hydrolysis of Mg-alkoxides. *Mater. Lett.* **2003**, *57*, 3998–4003. [CrossRef]

148. Karuppusamy, I.; Samuel, M.S.; Selvarajan, E.; Shanmugam, S.; Sahaya Murphin Kumar, P.; Brindhadevi, K.; Pugazhendhi, A. Ultrasound-assisted synthesis of mixed calcium magnesium oxide (CaMgO$_2$) nanoflakes for photocatalytic degradation of methylene blue. *J. Colloid Interface Sci.* **2021**, *584*, 770–778. [CrossRef]

149. Possato, L.G.; Gonçalves, R.G.L.; Santos, R.M.M.; Chaves, T.F.; Briois, V.; Pulcinelli, S.H.; Martins, L.; Santilli, C.V. Sol-gel synthesis of nanocrystalline MgO and its application as support in Ni/MgO catalysts for ethanol steam reforming. *Appl. Surf. Sci.* **2021**, *542*, 148744. [CrossRef]

150. Possato, L.G.; Pereira, E.; Gonçalves, R.G.L.; Pulcinelli, S.H.; Martins, L.; Santilli, C.V. Controlling the porosity and crystallinity of MgO catalysts by addition of surfactant in the sol-gel synthesis. *Catal. Today* **2020**, *344*, 52–58. [CrossRef]

151. Dong, B.; Qin, W.; Su, Y.; Wang, X. Magnetic properties of FeSiCr@MgO soft magnetic composites prepared by magnesium acetate pyrolysis for high-frequency applications. *J. Magn. Magn. Mater.* **2021**, *539*, 168350. [CrossRef]

152. Barati Dalenjan, M.; Rashidi, A.; Khorasheh, F.; Ardjmand, M. Effect of Ni ratio on mesoporous Ni/MgO nanocatalyst synthesized by one-step hydrothermal method for thermal catalytic decomposition of CH4 to H2. *Int. J. Hydrogen Energy* **2022**, *47*, 11539–11551. [CrossRef]

153. Sherikar, B.N.; Sahoo, B.; Umarji, A.M. Effect of fuel and fuel to oxidizer ratio in solution combustion synthesis of nanoceramic powders: MgO, CaO and ZnO. *Solid State Sci.* **2020**, *109*, 106426. [CrossRef]

154. Rao, L.S.; Rao, T.V.; Naheed, S.; Rao, P.V. Structural and optical properties of zinc magnesium oxide nanoparticles synthesized by chemical co-precipitation. *Mater. Chem. Phys.* **2018**, *203*, 133–140. [CrossRef]

155. Rajendran, V.; Deepa, B.; Mekala, R. Studies on structural, morphological, optical and antibacterial activity of Pure and Cu-doped MgO nanoparticles synthesized by co-precipitation method. *Mater. Today Proc.* **2018**, *5*, 8796–8803. [CrossRef]

156. Borgohain, X.; Boruah, A.; Sarma, G.K.; Rashid, M.H. Rapid and extremely high adsorption performance of porous MgO nanostructures for fluoride removal from water. *J. Mol. Liq.* **2020**, *305*, 112799. [CrossRef]

157. Lei, P.; Ding, X.; Bai, Y.; Yu, X.; Jiang, G.; Li, T.; Sun, B.; Zhang, X.; Li, X.; Wu, L.; et al. 1.8-μm MgO: PPLN optical parametric oscillator pumped by Nd: YVO4/YVO4 2nd-Stokes Raman laser. *Results Phys.* **2021**, *29*, 104703. [CrossRef]

158. Huang, S.; Kang, B.; Duan, L.; Zhang, D. Highly efficient inverted polymer solar cells by using solution processed MgO/ZnO composite interfacial layers. *J. Colloid Interface Sci.* **2021**, *583*, 178–187. [CrossRef]

159. Chetankumar, K.; Swamy, B.E.K.; Naik, H.S.B. MgO and MWCNTs amplified electrochemical sensor for guanine, adenine and epinephrine. *Mater. Chem. Phys.* **2021**, *267*, 124610. [CrossRef]

160. Sakoda, M.; Aibara, M.; Mede, K.; Kikuchi, M.; Naito, M. Superconducting tunnel junctions on MgB2 using MgO and CaF2 as a barrier. *Phys. C Supercond. Its Appl.* **2016**, *530*, 82–86. [CrossRef]

161. Guo, T.; Bulin, C. Facile fabrication of MgO/graphene oxide composite as an efficient adsorbent for rapid removal of aqueous organic dyes: Performance evaluation and mechanistic investigation. *J. Phys. Chem. Solids* **2021**, *158*, 110251. [CrossRef]

162. Nga, N.K.; Thuy Chau, N.T.; Viet, P.H. Preparation and characterization of a chitosan/MgO composite for the effective removal of reactive blue 19 dye from aqueous solution. *J. Sci. Adv. Mater. Devices* **2020**, *5*, 65–72. [CrossRef]

163. Cai, Y.; Li, C.; Wu, D.; Wang, W.; Tan, F.; Wang, X.; Wong, P.K.; Qiao, X. Highly active MgO nanoparticles for simultaneous bacterial inactivation and heavy metal removal from aqueous solution. *Chem. Eng. J.* **2017**, *312*, 158–166. [CrossRef]

164. Prado, D.C.; Fernández, I.; Rodríguez-Páez, J.E. MgO nanostructures: Synthesis, characterization and tentative mechanisms of nanoparticles formation. *Nano-Struct. Nano-Objects* **2020**, *23*, 100482. [CrossRef]

165. Yang, D.; Xu, P.; Guan, E.; Browning, N.D.; Gates, B.C. Rhodium pair-sites on magnesium oxide: Synthesis, characterization, and catalysis of ethylene hydrogenation. *J. Catal.* **2016**, *338*, 12–20. [CrossRef]

166. Maruthai, J.; Ramachandran, K.; Muthukumarasamy, A.; Chidambaram, S.; Gaidi, M.; Dauodi, K. Bio fabrication of 2D MgO/Ag nanocomposite for effective environmental utilization in antibacterial, anti-oxidant and catalytic applications. *Surf. Interfaces* **2022**, *30*, 101921. [CrossRef]

167. Dong, H.; Liu, M.; Yan, X.; Liu, M.; Qian, Z.; Xie, Y.; Luo, W.; Lei, C.; Zhou, Z. Pyrolysis gas from biomass and plastics over X-Mo@MgO (X = Ni, Fe, Co) catalysts into functional carbon nanocomposite: Gas reforming reaction and proper process mechanisms. *Sci. Total Environ.* **2022**, *831*, 154751. [CrossRef]

168. Sharmin, F.; Chandra Roy, D.; Basith, M.A. Photocatalytic water splitting ability of Fe/MgO-rGO nanocomposites towards hydrogen evolution. *Int. J. Hydrogen Energy* **2021**, *46*, 38232–38246. [CrossRef]

169. Shao, Y.; Zhao, D.-Y.; Lu, W.; Long, Y.; Zheng, W.; Zhao, J.; Hu, Z.-T. MgO/Carbon nanocomposites synthesized in molten salts for catalytic isomerization of glucose to fructose in aqueous media. *Green Chem. Eng.* **2021**, *3*, 359–366. [CrossRef]

170. Hamidian, K.; Saberian, M.R.; Miri, A.; Sharifi, F.; Sarani, M. Doped and un-doped cerium oxide nanoparticles: Biosynthesis, characterization, and cytotoxic study. *Ceram. Int.* **2021**, *47*, 13895–13902. [CrossRef]

171. Sebastiammal, S.; Bezy, N.A.; Somaprabha, A.; Henry, J.; Biju, C.S.; Fathima, A.L. Chemical and sweet basil leaf mediated synthesis of cerium oxide (CeO$_2$) nanoparticles: Antibacterial action toward human pathogens. *Phosphorus Sulfur Silicon Relat. Elem.* **2022**, *197*, 237–243. [CrossRef]

172. He, L.; Su, Y.; Lanhong, J.; Shi, S. Recent advances of cerium oxide nanoparticles in synthesis, luminescence and biomedical studies: A review. *J. Rare Earths* **2015**, *33*, 791–799. [CrossRef]

173. Niemiec, S.M.; Hilton, S.A.; Wallbank, A.; Azeltine, M.; Louiselle, A.E.; Elajaili, H.; Allawzi, A.; Xu, J.; Mattson, C.; Dewberry, L.C.; et al. Cerium oxide nanoparticle delivery of microRNA-146a for local treatment of acute lung injury. *Nanomed. Nanotechnol. Biol. Med.* **2021**, *34*, 102388. [CrossRef]

174. Asgharzadeh, F.; Hashemzadeh, A.; Rahmani, F.; Yaghoubi, A.; Nazari, S.E.; Avan, A.; Mehr, S.M.H.; Soleimanpour, S.; Khazaei, M. Cerium oxide nanoparticles acts as a novel therapeutic agent for ulcerative colitis through anti-oxidative mechanism. *Life Sci.* **2021**, *278*, 119500. [CrossRef] [PubMed]

175. Hasanzadeh, L.; Darroudi, M.; Ramezanian, N.; Zamani, P.; Aghaee-Bakhtiari, S.H.; Nourmohammadi, E.; Kazemi Oskuee, R. Polyethylenimine-associated cerium oxide nanoparticles: A novel promising gene delivery vector. *Life Sci.* **2019**, *232*, 116661. [CrossRef] [PubMed]

176. Wan, G.X.; Feng, Y.; Zhang, F.F.; Sun, X.W.; Li, Y.X.; Xue, R.J. Hydrothermal synthesis of Ag doped ZnO/CeO$_2$ nanocomposites and its application in ethanol sensing. *Mater. Lett.* **2022**, *318*, 132191. [CrossRef]

177. Negi, K.; Kumar, M.; Singh, G.; Chauhan, S.; Chauhan, M.S. Nanostructured CeO$_2$ for selective-sensing and smart photocatalytic applications. *Ceram. Int.* **2018**, *44*, 15281–15289. [CrossRef]

178. Veeresha, G.; Krishnamurthy, G.; Shivakumar, M.S. Cobalt nanocrystals doped on CeO$_2$/RGO nanocomposite for supercapacitor applications. *Inorg. Chem. Commun.* **2022**, *138*, 109232. [CrossRef]

179. Miller, H.A.; Bellini, M.; Dekel, D.R.; Vizza, F. Recent developments in Pd-CeO$_2$ nano-composite electrocatalysts for anodic reactions in anion exchange membrane fuel cells. *Electrochem. Commun.* **2022**, *135*, 107219. [CrossRef]

180. Wang, P.; Cai, C.; Tan, J.; Pan, M. Effect of the CeO$_2$ nanoparticles in microporous layers on the durability of proton exchange membrane fuel cells. *Int. J. Hydrogen Energy* **2021**, *46*, 34867–34873. [CrossRef]

181. Li, C.-M.; Zhang, Y.-S.; Wang, X.-P.; Yin, X.-B.; Luo, N.-N.; Khayambashi, A.; Wei, Y.-Z. The synthesis and characterization of hydrous cerium oxide nanoparticles loaded on porous silica micro-sphere as novel and efficient adsorbents to remove phosphate radicals from water. *Microporous Mesoporous Mater.* **2019**, *279*, 73–81. [CrossRef]

182. Yu, Y.; Zhang, C.; Yang, L.; Paul Chen, J. Cerium oxide modified activated carbon as an efficient and effective adsorbent for rapid uptake of arsenate and arsenite: Material development and study of performance and mechanisms. *Chem. Eng. J.* **2017**, *315*, 630–638. [CrossRef]

183. Bansal, R.; Nair, S.; Pandey, K.K. UV resistant wood coating based on zinc oxide and cerium oxide dispersed linseed oil nano-emulsion. *Mater. Today Commun.* **2022**, *30*, 103177. [CrossRef]

184. Gayathri, R.; Raja, G.; Rajeswaran, P. A simple and one step low cost microwave induced low cost grapheme modified CeO$_2$ photo electrodes for high-efficiency dye-sensitized solar cells. *Inorg. Chem. Commun.* **2020**, *120*, 108132. [CrossRef]

185. Latha, P.; Prakash, K.; Karuthapandian, S. Effective Photodegradation of CR & MO dyes by morphologically controlled Cerium oxide nanocubes under visible light Illumination. *Optik* **2018**, *154*, 242–250. [CrossRef]

186. Abbasi, M.A.; Amin, K.M.; Ali, M.; Ali, Z.; Atif, M.; Ensinger, W.; Khalid, W. Synergetic effect of adsorption-photocatalysis by GO−CeO2nanocomposites for photodegradation of doxorubicin. *J. Environ. Chem. Eng.* **2022**, *10*, 107078. [CrossRef]

187. Iqbal, A.; Ahmed, A.S.; Ahmad, N.; Shafi, A.; Ahamad, T.; Khan, M.Z.; Srivastava, S. Biogenic synthesis of CeO$_2$ nanoparticles and its potential application as an efficient photocatalyst for the degradation of toxic amido black dye. *Environ. Nanotechnol. Monit. Manag.* **2021**, *16*, 100505. [CrossRef]

188. Fang, X.; Song, H. Synthesis of cerium oxide nanoparticles loaded on chitosan for enhanced auto-catalytic regenerative ability and biocompatibility for the spinal cord injury repair. *J. Photochem. Photobiol. B Biol.* **2019**, *191*, 83–87. [CrossRef]

189. Mazloum-Ardakani, M.; Mohammadian-Sarcheshmeh, H.; Naderi, H.; Farbod, F.; Sabaghian, F. Fabrication of a high-performance hybrid supercapacitor using a modified graphene aerogel/cerium oxide nanoparticle composite. *J. Energy Storage* **2019**, *26*, 100998. [CrossRef]

190. Sridharan, M.; Kamaraj, P.; Vennilaraj; Arockiaselvi, J.; Pushpamalini, T.; Vivekanand, P.A.; Hari Kumar, S. Synthesis, characterization and evaluation of biosynthesized Cerium oxide nanoparticle for its anticancer activity on breast cancer cell (MCF 7). *Mater. Today Proc.* **2021**, *36*, 914–919. [CrossRef]

191. Shekunova, T.O.; Lapkina, L.A.; Shcherbakov, A.B.; Meshkov, I.N.; Ivanov, V.K.; Tsivadze, A.Y.; Gorbunova, Y.G. Deactivation of singlet oxygen by cerium oxide nanoparticles. *J. Photochem. Photobiol. A Chem.* **2019**, *382*, 111925. [CrossRef]

192. Selvaraj Janaki, N.J.; Ivan Jebakumar, D.S.; Sumithraj Premkumar, P. Studies on the physical properties of green synthesized cerium oxide nanoparticles using Melia dubia leaf extract. *Mater. Today Proc.* **2021**, *58*, 850–854. [CrossRef]

193. Hancock, M.L.; Yokel, R.A.; Beck, M.J.; Calahan, J.L.; Jarrells, T.W.; Munson, E.J.; Olaniyan, G.A.; Grulke, E.A. The characterization of purified citrate-coated cerium oxide nanoparticles prepared via hydrothermal synthesis. *Appl. Surf. Sci.* **2021**, *535*, 147681. [CrossRef]

194. Celardo, I.; Traversa, E.; Ghibelli, L. Cerium oxide nanoparticles: A promise for applications in therapy. *J. Exp. Ther. Oncol.* **2011**, *9*, 47–51. [PubMed]

195. Orge, C.A.; Órfão, J.J.M.; Pereira, M.F.R.; Duarte de Farias, A.M.; Neto, R.C.R.; Fraga, M.A. Ozonation of model organic compounds catalysed by nanostructured cerium oxides. *Appl. Catal. B Environ.* **2011**, *103*, 190–199. [CrossRef]

196. Akbari, A.; Khammar, M.; Taherzadeh, D.; Rajabian, A.; Khorsand Zak, A.; Darroudi, M. Zinc-doped cerium oxide nanoparticles: Sol-gel synthesis, characterization, and investigation of their in vitro cytotoxicity effects. *J. Mol. Struct.* **2017**, *1149*, 771–776. [CrossRef]

197. Muthuvel, A.; Jothibas, M.; Mohana, V.; Manoharan, C. Green synthesis of cerium oxide nanoparticles using Calotropis procera flower extract and their photocatalytic degradation and antibacterial activity. *Inorg. Chem. Commun.* **2020**, *119*, 108086. [CrossRef]

198. Syed Khadar, Y.A.; Balamurugan, A.; Devarajan, V.P.; Subramanian, R.; Dinesh Kumar, S. Synthesis, characterization and antibacterial activity of cobalt doped cerium oxide (CeO_2:Co) nanoparticles by using hydrothermal method. *J. Mater. Res. Technol.* **2019**, *8*, 267–274. [CrossRef]

199. Kishor Kumar, M.J.; Kalathi, J.T. Low-temperature sonochemical synthesis of high dielectric Lanthanum doped Cerium oxide nanopowder. *J. Alloys Compd.* **2018**, *748*, 348–354. [CrossRef]

200. Soren, S.; Bessoi, M.; Parhi, P. A rapid microwave initiated polyol synthesis of cerium oxide nanoparticle using different cerium precursors. *Ceram. Int.* **2015**, *41*, 8114–8118. [CrossRef]

201. Ahmed, S.H.; Bakiro, M.; Aljasmi, F.I.A.; Albreiki, A.M.O.; Bayane, S.; Alzamly, A. Investigation of the band gap and photocatalytic properties of CeO_2/rGO composites. *Mol. Catal.* **2020**, *486*, 110874. [CrossRef]

202. Faghihinezhad, M.; Baghdadi, M.; Shahin, M.S.; Torabian, A. Catalytic ozonation of real textile wastewater by magnetic oxidized g-C3N4 modified with Al_2O_3 nanoparticles as a novel catalyst. *Sep. Purif. Technol.* **2022**, *283*, 120208. [CrossRef]

203. Bahari, M.B.; Mamat, C.R.; Jalil, A.A.; Hassan, N.S.; Nabgan, W.; Setiabudi, H.D.; Vo, D.-V.N.; Phuong Thuy, B.T. Mesoporous alumina: A comprehensive review on synthesis strategies, structure, and applications as support for enhanced H2 generation via CO2-CH4 reforming. *Int. J. Hydrogen Energy* **2022**, *47*, 41507–41526. [CrossRef]

204. Contreras, J.E.; Taha-Tijerina, J.; López-Perales, J.F.; Banda-Muñoz, F.; Díaz-Tato, L.; Rodríguez, E.A. Enhancing the quartz-clay-feldspar system by nano-Al_2O_3 addition for electrical insulators: From laboratory to prototype scale. *Mater. Chem. Phys.* **2021**, *263*, 124389. [CrossRef]

205. Chang, Y.-J.; Xie, G.-H.; Zhou, Y.-M.; Wang, J.-X.; Wang, Z.-X.; Guo, H.-J.; You, B.-Z.; Yan, G.-C. Enhancing storage performance of P2-type Na2/3Fe1/2Mn1/2O2 cathode materials by Al_2O_3 coating. *Trans. Nonferrous Met. Soc. China* **2022**, *32*, 262–272. [CrossRef]

206. Khaleduzzaman, S.S.; Sohel, M.R.; Saidur, R.; Selvaraj, J. Stability of Al_2O_3-water Nanofluid for Electronics Cooling System. *Procedia Eng.* **2015**, *105*, 406–411. [CrossRef]

207. Goyal, R.K.; Tiwari, A.N.; Mulik, U.P.; Negi, Y.S. Novel high performance Al_2O_3/poly(ether ether ketone) nanocomposites for electronics applications. *Compos. Sci. Technol.* **2007**, *67*, 1802–1812. [CrossRef]

208. Moutcine, A.; Ifguis, O.; Amine Samaini, M.; Ennachete, M.; Sâadane, H.; Laghlimi, C.; Chtaini, A. Simultaneous electrochemical determination of heavy metals by an electrode modified CPE-NP-Al2O3. *Mater. Today Proc.* **2022**, *53*, 404–407. [CrossRef]

209. Saadi, Z.; Saadi, R.; Fazaeli, R. Fixed-bed adsorption dynamics of Pb (II) adsorption from aqueous solution using nanostructured γ-alumina. *J. Nanostruct. Chem.* **2013**, *3*, 48. [CrossRef]

210. Liu, X.; Niu, C.; Zhen, X.; Wang, J.; Su, X. Novel approach for synthesis of boehmite nanostructures and their conversion to aluminum oxide nanostructures for remove Congo red. *J. Colloid Interface Sci.* **2015**, *452*, 116–125. [CrossRef]

211. Hossain, A.M.S.; Balbín, A.; Erami, R.S.; Prashar, S.; Fajardo, M.; Gómez-Ruiz, S. Synthesis and study of the catalytic applications in C–C coupling reactions of hybrid nanosystems based on alumina and palladium nanoparticles. *Inorg. Chim. Acta* **2017**, *455*, 645–652. [CrossRef]

212. Tan, H.-b.; Guo, C.-s. Preparation of long alumina fibers by sol-gel method using malic acid. *Trans. Nonferrous Met. Soc. China* **2011**, *21*, 1563–1567. [CrossRef]

213. Tzompantzi, F.; Piña, Y.; Mantilla, A.; Aguilar-Martínez, O.; Galindo-Hernández, F.; Bokhimi, X.; Barrera, A. Hydroxylated sol–gel Al_2O_3 as photocatalyst for the degradation of phenolic compounds in presence of UV light. *Catal. Today* **2014**, *220–222*, 49–55. [CrossRef]

214. Piña-Pérez, Y.; Tzompantzi-Morales, F.; Pérez-Hernández, R.; Arroyo-Murillo, R.; Acevedo-Peña, P.; Gómez-Romero, R. Photocatalytic activity of Al_2O_3 improved by the addition of Ce^{3+}/Ce^{4+} synthesized by the sol-gel method. Photodegradation of phenolic compounds using UV light. *Fuel* **2017**, *198*, 11–21. [CrossRef]

215. Polat Gonullu, M. Design and characterization of single bilayer ZnO/Al_2O_3 film by ultrasonically spray pyrolysis and its application in photocatalysis. *Superlattices Microstruct.* **2021**, *164*, 107113. [CrossRef]

216. Tan, L.; Dong, W.; Liu, K.; Luo, T.; Gu, X. Thermal decomposition in-situ preparation of gray rutile TiO_{2-x}/Al_2O_3 composite and its enhanced visible-light-driven photocatalytic properties. *Opt. Mater.* **2021**, *111*, 110716. [CrossRef]

217. Veksha, A.; Bin Mohamed Amrad, M.Z.; Chen, W.Q.; Binte Mohamed, D.K.; Tiwari, S.B.; Lim, T.-T.; Lisak, G. Tailoring Fe_2O_3–Al_2O_3 catalyst structure and activity via hydrothermal synthesis for carbon nanotubes and hydrogen production from polyolefin plastics. *Chemosphere* **2022**, *297*, 134148. [CrossRef] [PubMed]

218. Chong, X.; Xiao, G.; Ding, D.; Luo, J.; Zheng, X. Combustion synthesis of $SiC/Al2O3$ composite powders with SiC nanowires and their growth mechanism. *Ceram. Int.* **2022**, *48*, 1778–1788. [CrossRef]

219. Rahbar Shamskar, F.; Meshkani, F.; Rezaei, M. Ultrasound assisted co-precipitation synthesis and catalytic performance of mesoporous nanocrystalline NiO-Al2O3 powders. *Ultrason. Sonochem.* **2017**, *34*, 436–447. [CrossRef]

220. Grishina, E.P.; Kudryakova, N.O.; Ramenskaya, L.M. Thin-film Al_2O_3 coating on low carbon steel obtained by the sol–gel method with different peptizing acids: Corrosion investigation. *Thin Solid Film.* **2022**, *746*, 139125. [CrossRef]

221. Mirjalili, F.; Mohamad, H.; Luqman Chuah, A. Preparation of nano-scale alpha-Al_2O_3 powder by the sol-gel method. *Ceram. Silik.* **2011**, *55*, 378–383.

222. Mavrič, A.; Valant, M.; Cui, C.; Wang, Z.M. Advanced applications of amorphous alumina: From nano to bulk. *J. Non-Cryst. Solids* **2019**, *521*, 119493. [CrossRef]

223. Peintinger, M.F.; Kratz, M.J.; Bredow, T. Quantum-chemical study of stable, meta-stable and high-pressure alumina polymorphs and aluminum hydroxides. *J. Mater. Chem. A* **2014**, *2*, 13143–13158. [CrossRef]

224. Mallakpour, S.; Khadem, E. Recent development in the synthesis of polymer nanocomposites based on nano-alumina. *Prog. Polym. Sci.* **2015**, *51*, 74–93. [CrossRef]

225. Niero, D.F.; Montedo, O.R.K.; Bernardin, A.M. Synthesis and characterization of nano α-alumina by an inorganic sol–gel method. *Mater. Sci. Eng. B* **2022**, *280*, 115690. [CrossRef]

226. Xiao, W.; Wang, D.; Lou, X.W. Shape-Controlled Synthesis of MnO_2 Nanostructures with Enhanced Electrocatalytic Activity for Oxygen Reduction. *J. Phys. Chem. C* **2010**, *114*, 1694–1700. [CrossRef]

227. Yan, D.; Yan, P.X.; Yue, G.H.; Liu, J.Z.; Chang, J.B.; Yang, Q.; Qu, D.M.; Geng, Z.R.; Chen, J.T.; Zhang, G.A.; et al. Self-assembled flower-like hierarchical spheres and nanobelts of manganese oxide by hydrothermal method and morphology control of them. *Chem. Phys. Lett.* **2007**, *440*, 134–138. [CrossRef]

228. Rao, B.C.N.R.; Govindaraj, A.; Vivekchand, S.R.C. Inorganic nanomaterials: Current status and future prospects. *Annu. Rep. Sect. A (Inorg. Chem.)* **2006**, *102*, 20–45. [CrossRef]

229. McKenzie, R.M. The synthesis of birnessite, cryptomelane, and some other oxides and hydroxides of manganese. *Mineral. Mag.* **2018**, *38*, 493–502. [CrossRef]

230. Shih, Y.-J.; Huang, R.; Huang, Y.H. Adsorptive removal of arsenic using a novel akhtenskite coated waste Goethite. *J. Clean. Prod.* **2015**, *87*, 897–905. [CrossRef]

231. Indra, A.; Menezes, P.W.; Schuster, F.; Driess, M. Significant role of Mn(III) sites in eg1 configuration in manganese oxide catalysts for efficient artificial water oxidation. *J. Photochem. Photobiol. B Biol.* **2015**, *152*, 156–161. [CrossRef]

232. Shin, J.; Seo, J.K.; Yaylian, R.; Huang, A.; Meng, Y.S. A review on mechanistic understanding of MnO_2 in aqueous electrolyte for electrical energy storage systems. *Int. Mater. Rev.* **2020**, *65*, 356–387. [CrossRef]

233. Juran, T.R.; Young, J.; Smeu, M. Density Functional Theory Modeling of MnO2 Polymorphs as Cathodes for Multivalent Ion Batteries. *J. Phys. Chem. C* **2018**, *122*, 8788–8795. [CrossRef]

234. Šťastný, M.; Stengl, V.; Henych, J.; Tolasz, J.; Vomáčka, P.; Ederer, J. Mesoporous manganese oxide for the degradation of organophosphates pesticides. *J. Mater. Sci.* **2016**, *51*, 2634–2642. [CrossRef]

235. Ebrahimi, R.; Mohammadi, M.; Maleki, A.; Jafari, A.; Shahmoradi, B.; Rezaee, R.; Safari, M.; Daraei, H.; Giahi, O.; Yetilmezsoy, K.; et al. Photocatalytic Degradation of 2,4-Dichlorophenoxyacetic Acid in Aqueous Solution Using Mn-doped ZnO/Graphene Nanocomposite Under LED Radiation. *J. Inorg. Organomet. Polym. Mater.* **2020**, *30*, 923–934. [CrossRef]

236. Zandsalimi, Y.; Maleki, A.; Shahmoradi, B.; Dehestani, S.; Rezaee, R.; McKay, G. Photocatalytic removal of 2,4-Dichlorophenoxyacetic acid from aqueous solution using tungsten oxide doped zinc oxide nanoparticles immobilised on glass beads. *Environ. Technol.* **2022**, *43*, 631–645. [CrossRef]

237. Maleki, A.; Moradi, F.; Shahmoradi, B.; Rezaee, R.; Lee, S.-M. The photocatalytic removal of diazinon from aqueous solutions using tungsten oxide doped zinc oxide nanoparticles immobilized on glass substrate. *J. Mol. Liq.* **2020**, *297*, 111918. [CrossRef]

238. Nagpal, M.; Kakkar, R. Use of metal oxides for the adsorptive removal of toxic organic pollutants. *Sep. Purif. Technol.* **2019**, *211*, 522–539. [CrossRef]

239. Sheela, T.; Nayaka, Y.A. Kinetics and thermodynamics of cadmium and lead ions adsorption on NiO nanoparticles. *Chem. Eng. J.* **2012**, *191*, 123–131. [CrossRef]

240. Ahmad Bhat, S.; Zafar, F.; Ullah Mirza, A.; Hossain Mondal, A.; Kareem, A.; Haq, Q.M.R.; Nishat, N. NiO nanoparticle doped-PVA-MF polymer nanocomposites: Preparation, Congo red dye adsorption and antibacterial activity. *Arab. J. Chem.* **2020**, *13*, 5724–5739. [CrossRef]

241. Pooyandeh, S.; Shahidi, S.; Khajehnezhad, A.; Mongkholrattanasit, R. In situ deposition of NiO nano particles on cotton fabric using sol–gel method- photocatalytic activation properties. *J. Mater. Res. Technol.* **2021**, *12*, 1–14. [CrossRef]

242. Ibrahim, E.M.M.; Abdel-Rahman, L.H.; Abu-Dief, A.M.; Elshafaie, A.; Hamdan, S.K.; Ahmed, A.M. The synthesis of CuO and NiO nanoparticles by facile thermal decomposition of metal-Schiff base complexes and an examination of their electric, thermoelectric and magnetic Properties. *Mater. Res. Bull.* **2018**, *107*, 492–497. [CrossRef]

243. Mohandesi, M.; Tavakolian, M.; Rahimpour, M.R. Eggplant as an appreciable bio-template for green synthesis of NiO nanoparticles: Study of physical and photocatalytic properties. *Ceram. Int.* **2022**, *48*, 22820–22826. [CrossRef]

244. Mostafa, A.M.; Mwafy, E.A. The effect of laser fluence for enhancing the antibacterial activity of NiO nanoparticles by pulsed laser ablation in liquid media. *Environ. Nanotechnol. Monit. Manag.* **2020**, *14*, 100382. [CrossRef]

245. Kumar, J.P.; Giri, S.D.; Sarkar, A. Mesoporous NiO with different morphology: Synthesis, characterization and their evaluation for oxygen evolution reaction. *Int. J. Hydrogen Energy* **2018**, *43*, 15639–15649. [CrossRef]

246. Hosny, N.M. Synthesis, characterization and optical band gap of NiO nanoparticles derived from anthranilic acid precursors via a thermal decomposition route. *Polyhedron* **2011**, *30*, 470–476. [CrossRef]

247. Rashidimoghaddam, M.; Saljooqi, A.; Shamspur, T.; Mostafavi, A. Constructing S-doped Ni–Co LDH intercalated with Fe_3O_4 heterostructure photocatalysts for enhanced pesticide degradation. *New J. Chem.* **2020**, *44*, 15584–15592. [CrossRef]

248. Gaya, U.I.; Abdullah, A.H. Heterogeneous photocatalytic degradation of organic contaminants over titanium dioxide: A review of fundamentals, progress and problems. *J. Photochem. Photobiol. C Photochem. Rev.* **2008**, *9*, 1–12. [CrossRef]

249. Hassaan, M.A.; El Nemr, A. Pesticides pollution: Classifications, human health impact, extraction and treatment techniques. *Egypt. J. Aquat. Res.* **2020**, *46*, 207–220. [CrossRef]

250. Abubakar, Y.; Tijjani, H.; Egbuna, C.; Adetunji, C.O.; Kala, S.; Kryeziu, T.L.; Ifemeje, J.C.; Patrick-Iwuanyanwu, K.C. Chapter 3—Pesticides, History, and Classification. In *Natural Remedies for Pest, Disease and Weed Control*; Egbuna, C., Sawicka, B., Eds.; Academic Press: Cambridge, MA, USA, 2020; pp. 29–42. [CrossRef]

251. Sousa, R.M.O.F.; Cunha, A.C.; Fernandes-Ferreira, M. The potential of Apiaceae species as sources of singular phytochemicals and plant-based pesticides. *Phytochemistry* **2021**, *187*, 112714. [CrossRef]

252. George, D.; Finn, R.; Graham, K.; Sparagano, O. Present and future potential of plant-derived products to control arthropods of veterinary and medical significance. *Parasites Vectors* **2014**, *7*, 28. [CrossRef]

253. Quijano, L.; Yusà, V.; Font, G.; Pardo, O. Chronic cumulative risk assessment of the exposure to organophosphorus, carbamate and pyrethroid and pyrethrin pesticides through fruit and vegetables consumption in the region of Valencia (Spain). *Food Chem. Toxicol.* **2016**, *89*, 39–46. [CrossRef]

254. Pirsaheb, M.; Fattahi, N.; Rahimi, R.; Sharafi, K.; Ghaffari, H.R. Evaluation of abamectin, diazinon and chlorpyrifos pesticide residues in apple product of Mahabad region gardens: Iran in 2014. *Food Chem.* **2017**, *231*, 148–155. [CrossRef]

255. Blankson, G.K.; Osei-Fosu, P.; Adeendze, E.A.; Ashie, D. Contamination levels of organophosphorus and synthetic pyrethroid pesticides in vegetables marketed in Accra, Ghana. *Food Control* **2016**, *68*, 174–180. [CrossRef]

256. Yuan, Y.; Chen, C.; Zheng, C.; Wang, X.; Yang, G.; Wang, Q.; Zhang, Z. Residue of chlorpyrifos and cypermethrin in vegetables and probabilistic exposure assessment for consumers in Zhejiang Province, China. *Food Control* **2014**, *36*, 63–68. [CrossRef]

257. Ciasca, B.; Pecorelli, I.; Lepore, L.; Paoloni, A.; Catucci, L.; Pascale, M.; Lattanzio, V.M.T. Rapid and reliable detection of glyphosate in pome fruits, berries, pulses and cereals by flow injection—Mass spectrometry. *Food Chem.* **2020**, *310*, 125813. [CrossRef] [PubMed]

258. Mojsak, P.; Łozowicka, B.; Kaczyński, P. Estimating acute and chronic exposure of children and adults to chlorpyrifos in fruit and vegetables based on the new, lower toxicology data. *Ecotoxicol. Environ. Saf.* **2018**, *159*, 182–189. [CrossRef] [PubMed]

259. Li, Z.; Zhang, Y.; Zhao, Q.; Wang, C.; Cui, Y.; Li, J.; Chen, A.; Liang, G.; Jiao, B. Occurrence, temporal variation, quality and safety assessment of pesticide residues on citrus fruits in China. *Chemosphere* **2020**, *258*, 127381. [CrossRef]

260. Hirano, T.; Suzuki, N.; Ikenaka, Y.; Hoshi, N.; Tabuchi, Y. Neurotoxicity of a pyrethroid pesticide deltamethrin is associated with the imbalance in proteolytic systems caused by mitophagy activation and proteasome inhibition. *Toxicol. Appl. Pharmacol.* **2021**, *430*, 115723. [CrossRef]

261. Nurdin, M.; Maulidiyah, M.; Salim, L.O.A.; Muzakkar, M.Z.; Umar, A.A. High performance cypermethrin pesticide detection using anatase TiO2-carbon paste nanocomposites electrode. *Microchem. J.* **2019**, *145*, 756–761. [CrossRef]

262. Xia, Y.; Bian, Q.; Xu, L.; Cheng, S.; Song, L.; Liu, J.; Wu, W.; Wang, S.; Wang, X. Genotoxic effects on human spermatozoa among pesticide factory workers exposed to fenvalerate. *Toxicology* **2004**, *203*, 49–60. [CrossRef]

263. Gupta, D.; Jamwal, D.; Rana, D.; Katoch, A. 26—Microwave synthesized nanocomposites for enhancing oral bioavailability of drugs. In *Applications of Nanocomposite Materials in Drug Delivery*; Inamuddin, A.M.A., Mohammad, A., Eds.; Woodhead Publishing: Cambridge, UK, 2018; pp. 619–632. [CrossRef]

264. Dabrowski, A. Adsorption–from theory to practice. *Adv Colloid Interface Sci* **2001**, *93*, 135–224. [CrossRef]

265. del Mar Orta, M.; Martín, J.; Medina-Carrasco, S.; Santos, J.L.; Aparicio, I.; Alonso, E. Adsorption of propranolol onto montmorillonite: Kinetic, isotherm and pH studies. *Appl. Clay Sci.* **2019**, *173*, 107–114. [CrossRef]

266. Derylo-Marczewska, A.; Blachnio, M.; Marczewski, A.W.; Swiatkowski, A.; Buczek, B. Adsorption of chlorophenoxy pesticides on activated carbon with gradually removed external particle layers. *Chem. Eng. J.* **2017**, *308*, 408–418. [CrossRef]

267. Sharma, L.; Kakkar, R. Hierarchically structured magnesium based oxides: Synthesis strategies and applications in organic pollutant remediation. *CrystEngComm* **2017**, *19*, 6913–6926. [CrossRef]

268. Batzill, M. Fundamental aspects of surface engineering of transition metal oxide photocatalysts. *Energy Environ. Sci.* **2011**, *4*, 3275–3286. [CrossRef]

269. Mahmoud, A.M.; Ibrahim, F.A.; Shaban, S.A.; Youssef, N.A. Adsorption of heavy metal ion from aqueous solution by nickel oxide nano catalyst prepared by different methods. *Egypt. J. Pet.* **2015**, *24*, 27–35. [CrossRef]

270. Crini, G.; Lichtfouse, E.; Wilson, L.D.; Morin-Crini, N. Adsorption-Oriented Processes Using Conventional and Non-conventional Adsorbents for Wastewater Treatment. In *Green Adsorbents for Pollutant Removal: Fundamentals and Design*; Crini, G., Lichtfouse, E., Eds.; Springer International Publishing: Cham, Switzerland, 2018; pp. 23–71. [CrossRef]

271. Králik, M. Adsorption, chemisorption, and catalysis. *Chem. Pap.* **2014**, *68*, 1625–1638. [CrossRef]

272. Edet, U.A.; Ifelebuegu, A.O. Kinetics, Isotherms, and Thermodynamic Modeling of the Adsorption of Phosphates from Model Wastewater Using Recycled Brick Waste. *Processes* **2020**, *8*, 665. [CrossRef]

273. Ahmed, M.J.; Hameed, B.H. Insights into the isotherm and kinetic models for the coadsorption of pharmaceuticals in the absence and presence of metal ions: A review. *J. Environ. Manag.* **2019**, *252*, 109617. [CrossRef]

274. Adeola, A.O.; Abiodun, B.A.; Adenuga, D.O.; Nomngongo, P.N. Adsorptive and photocatalytic remediation of hazardous organic chemical pollutants in aqueous medium: A review. *J. Contam. Hydrol.* **2022**, *248*, 104019. [CrossRef]

275. Salam, M.A.; AbuKhadra, M.R.; Mohamed, A.S. Effective oxidation of methyl parathion pesticide in water over recycled glass based-MCM-41 decorated by green Co3O4 nanoparticles. *Environ. Pollut.* **2020**, *259*, 113874. [CrossRef]

276. Zhao, J.; Huang, P.; Wang, X.; Yang, J.; Zhou, Z.; Du, X.; Lu, X. Efficient adsorption removal of organic nitrogen pesticides: Insight into a new hollow NiO/Co@C magnetic nanocomposites derived from metal-organic framework. *Sep. Purif. Technol.* **2022**, *287*, 120608. [CrossRef]

277. Abdelillah Ali Elhussein, E.; Şahin, S.; Bayazit, Ş.S. Preparation of CeO$_2$ nanofibers derived from Ce-BTC metal-organic frameworks and its application on pesticide adsorption. *J. Mol. Liq.* **2018**, *255*, 10–17. [CrossRef]

278. Zhou, D.-D.; Lu, Z.-H.; Chen, M.; Zhuang, L.-Y.; Cao, Y.-W.; Liu, X.; Senosy, I.A.; Yang, Z.-H. A novel magnetic double MOF composite is synthesized for removing azole fungicides economically and efficiently. *Appl. Surf. Sci.* **2022**, *594*, 153441. [CrossRef]

279. Sharma, L.; Kakkar, R. Magnetically retrievable one-pot fabrication of mesoporous magnesium ferrite (MgFe$_2$O$_4$) for the remediation of chlorpyrifos and real pesticide wastewater. *J. Environ. Chem. Eng.* **2018**, *6*, 6891–6903. [CrossRef]

280. Nayak, A.; Bhushan, B.; Sharma, P.K.; Gupta, V. Development of Magnetic Nanoparticles from Poplar Sawdust for Removal of Pesticides from Aqueous Solution. *J. Graph. Era Univ.* **2018**, *6*, 55–70.

281. Kaur, Y.; Bhatia, Y.; Chaudhary, S.; Chaudhary, G.R. Comparative performance of bare and functionalize ZnO nanoadsorbents for pesticide removal from aqueous solution. *J. Mol. Liq.* **2017**, *234*, 94–103. [CrossRef]

282. Chen, D.; Chen, C.; Shen, W.; Quan, H.; Chen, S.; Xie, S.; Luo, X.; Guo, L. MOF-derived magnetic porous carbon-based sorbent: Synthesis, characterization, and adsorption behavior of organic micropollutants. *Adv. Powder Technol.* **2017**, *28*, 1769–1779. [CrossRef]

283. Cao, X.; Liu, G.; She, Y.; Jiang, Z.; Jin, F.; Jin, M.; Du, P.; Zhao, F.; Zhang, Y.; Wang, J. Preparation of magnetic metal organic framework composites for the extraction of neonicotinoid insecticides from environmental water samples. *RSC Adv.* **2016**, *6*, 113144–113151. [CrossRef]

284. Su, H.; Lin, Y.; Wang, Z.; Wong, Y.L.; Chen, X.; Chan, T.W. Magnetic metal-organic framework-titanium dioxide nanocomposite as adsorbent in the magnetic solid-phase extraction of fungicides from environmental water samples. *J. Chromatogr. A* **2016**, *1466*, 21–28. [CrossRef]

285. Liu, G.; Li, L.; Huang, X.; Zheng, S.; Xu, D.; Xu, X.; Zhang, Y.; Lin, H. Determination of triazole pesticides in aqueous solution based on magnetic graphene oxide functionalized MOF-199 as solid phase extraction sorbents. *Microporous Mesoporous Mater.* **2018**, *270*, 258–264. [CrossRef]

286. Liu, G.; Li, L.; Huang, X.; Zheng, S.; Xu, X.; Liu, Z.; Zhang, Y.; Wang, J.; Lin, H.; Xu, D. Adsorption and removal of organophosphorus pesticides from environmental water and soil samples by using magnetic multi-walled carbon nanotubes @ organic framework ZIF-8. *J. Mater. Sci.* **2018**, *53*, 10772–10783. [CrossRef]

287. Badawy, M.E.I.; El-Nouby, M.A.M.; Marei, A.E.-S.M. Development of a Solid-Phase Extraction (SPE) Cartridge Based on Chitosan-Metal Oxide Nanoparticles (Ch-MO NPs) for Extraction of Pesticides from Water and Determination by HPLC. *Int. J. Anal. Chem.* **2018**, *2018*, 3640691. [CrossRef] [PubMed]

288. Moradi Dehaghi, S.; Rahmanifar, B.; Moradi, A.M.; Azar, P.A. Removal of permethrin pesticide from water by chitosan–zinc oxide nanoparticles composite as an adsorbent. *J. Saudi Chem. Soc.* **2014**, *18*, 348–355. [CrossRef]

289. Parsaie, A.; Rahbar, N.; Baezat, M. A New Fe$_3$O$_4$/CuO/AC Nanocomposite for Imidacloprid Removal: Characterization, Optimization, and Adsorption Modeling. *Res. Sq.* **2021**. [CrossRef]

290. ul Haq, A.; Saeed, M.; Usman, M.; Naqvi, S.A.R.; Bokhari, T.H.; Maqbool, T.; Ghaus, H.; Tahir, T.; Khalid, H. Sorption of chlorpyrifos onto zinc oxide nanoparticles impregnated Pea peels (*Pisum sativum* L): Equilibrium, kinetic and thermodynamic studies. *Environ. Technol. Innov.* **2020**, *17*, 100516. [CrossRef]

291. Haq, A.; Saeed, M.; Muneer, M.; Jamal, M.; Maqbool, T.; Tahir, T. Biosorption of metribuzin pesticide by Cucumber (*Cucumis sativus*) peels-zinc oxide nanoparticles composite. *Sci. Rep.* **2022**, *12*, 5840. [CrossRef]

292. Cusioli, L.F.; Quesada, H.B.; Barbosa de Andrade, M.; Gomes, R.G.; Bergamasco, R. Application of a novel low-cost adsorbent functioned with iron oxide nanoparticles for the removal of triclosan present in contaminated water. *Microporous Mesoporous Mater.* **2021**, *325*, 111328. [CrossRef]

293. Allam, E.A.; Ali, A.S.M.; Elsharkawy, R.M.; Mahmoud, M.E. Framework of nano metal oxides N-NiO@N-Fe$_3$O$_4$@N-ZnO for adsorptive removal of atrazine and bisphenol-A from wastewater: Kinetic and adsorption studies. *Environ. Nanotechnol. Monit. Manag.* **2021**, *16*, 100481. [CrossRef]

294. Rao, T.N.; Balaji, A.P.B.; Panagal, M.; Parvatamma, B.; Selvaraj, B.; Panneerselvam, S.; Aruni, W.; Subramanian, K.; Sampath Renuga, P.; Pandian, S. Nanoremediation of dimethomorph in water samples using magnesium aluminate nanoparticles. *Environ. Technol. Innov.* **2020**, *20*, 101176. [CrossRef]

295. Lan, J.; Cheng, Y.; Zhao, Z. Effective organochlorine pesticides removal from aqueous systems by magnetic nanospheres coated with polystyrene. *J. Wuhan Univ. Technol.-Mater. Sci. Ed.* **2014**, *29*, 168–173. [CrossRef]

296. Armaghan, M.; Amini, M.M. Adsorption of diazinon and fenitrothion on nanocrystalline magnesium oxides. *Arab. J. Chem.* **2017**, *10*, 91–99. [CrossRef]

297. Liu, F.; Tian, H.; He, J. Adsorptive performance and catalytic activity of superparamagnetic Fe3O4@nSiO2@mSiO2 core–shell microspheres towards DDT. *J. Colloid Interface Sci.* **2014**, *419*, 68–72. [CrossRef] [PubMed]

298. Vaya, D.; Surolia, P.K. Semiconductor based photocatalytic degradation of pesticides: An overview. *Environ. Technol. Innov.* **2020**, *20*, 101128. [CrossRef]

299. Krishnasamy, L.; Krishna, K.; Subpiramaniyam, S. Photocatalytic Degradation of Atrazine in Aqueous Solution Using La-Doped ZnO/PAN Nanofibers. *Environ. Sci. Pollut. Res.* **2022**, *29*, 54282–54291. [CrossRef]

300. Rani, M.; Yadav, J.; Keshu; Shanker, U. Green synthesis of sunlight responsive zinc oxide coupled cadmium sulfide nanostructures for efficient photodegradation of pesticides. *J. Colloid Interface Sci.* **2021**, *601*, 689–703. [CrossRef]

301. Zhu, Z.; Guo, F.; Xu, Z.; Di, X.; Zhang, Q. Photocatalytic degradation of an organophosphorus pesticide using a ZnO/rGO composite. *RSC Adv.* **2020**, *10*, 11929–11938. [CrossRef]

302. Anirudhan, T.S.; Shainy, F.; Sekhar, V.C.; Athira, V.S. Highly efficient photocatalytic degradation of chlorpyrifos in aqueous solutions by nano hydroxyapatite modified CFGO/ZnO nanorod composite. *J. Photochem. Photobiol. A Chem.* **2021**, *418*, 113333. [CrossRef]

303. Soltani-nezhad, F.; Saljooqi, A.; Shamspur, T.; Mostafavi, A. Photocatalytic degradation of imidacloprid using GO/Fe$_3$O$_4$/TiO$_2$-NiO under visible radiation: Optimization by response level method. *Polyhedron* **2019**, *165*, 188–196. [CrossRef]

304. Zangiabadi, M.; Shamspur, T.; Saljooqi, A.; Mostafavi, A. Evaluating the efficiency of the GO-Fe$_3$O$_4$/TiO$_2$ mesoporous photocatalyst for degradation of chlorpyrifos pesticide under visible light irradiation. *Appl. Organomet. Chem.* **2019**, *33*, e4813. [CrossRef]

305. Andronic, L.; Vladescu, A.; Enesca, A. Synthesis, Characterisation, Photocatalytic Activity, and Aquatic Toxicity Evaluation of TiO$_2$ Nanoparticles. *Nanomaterials* **2021**, *11*, 3197. [CrossRef] [PubMed]

306. Čižmar, T.; Panžić, I.; Capan, I.; Gajović, A. Nanostructured TiO$_2$ photocatalyst modified with Cu for improved imidacloprid degradation. *Appl. Surf. Sci.* **2021**, *569*, 151026. [CrossRef]

307. Khan, S.H.; Pathak, B. Zinc oxide based photocatalytic degradation of persistent pesticides: A comprehensive review. *Environ. Nanotechnol. Monit. Manag.* **2020**, *13*, 100290. [CrossRef]

308. AbuKhadra, M.R.; Mohamed, A.S.; El-Sherbeeny, A.M.; Elmeligy, M.A. Enhanced photocatalytic degradation of acephate pesticide over MCM-41/Co3O4 nanocomposite synthesized from rice husk silica gel and Peach leaves. *J. Hazard. Mater.* **2020**, *389*, 122129. [CrossRef]

309. Mohamed, A.S.; Abukkhadra, M.R.; Abdallah, E.A.; El-Sherbeeny, A.M.; Mahmoud, R.K. The photocatalytic performance of silica fume based Co3O4/MCM-41 green nanocomposite for instantaneous degradation of Omethoate pesticide under visible light. *J. Photochem. Photobiol. A Chem.* **2020**, *392*, 112434. [CrossRef]

310. Hanh, N.T.; Le Minh Tri, N.; Van Thuan, D.; Thanh Tung, M.H.; Pham, T.-D.; Minh, T.D.; Trang, H.T.; Binh, M.T.; Nguyen, M.V. Monocrotophos pesticide effectively removed by novel visible light driven Cu doped ZnO photocatalyst. *J. Photochem. Photobiol. A Chem.* **2019**, *382*, 111923. [CrossRef]

311. Kumari, V.; Sharma, S.; Sharma, A.; Kumari, K.; Kumar, N. Hydrothermal synthesis conditions effect on hierarchical ZnO/CuO hybrid materials and their photocatalytic activity. *J. Mater. Sci. Mater. Electron.* **2021**, *32*, 9596–9610. [CrossRef]

312. Iqbal, A.; Haq, A.u.; Cerrón-Calle, G.A.; Naqvi, S.A.R.; Westerhoff, P.; Garcia-Segura, S. Green synthesis of flower-shaped copper oxide and nickel oxide nanoparticles via capparis decidua leaf extract for synergic adsorption-photocatalytic degradation of pesticides. *Catalysts* **2021**, *11*, 806. [CrossRef]

313. Aguilera-Ruiz, E.; De La Garza-Galván, M.; Zambrano-Robledo, P.; Ballesteros-Pacheco, J.C.; Vazquez-Arenas, J.; Peral, J.; García-Pérez, U.M. Facile synthesis of visible-light-driven Cu$_2$O/BiVO$_4$ composites for the photomineralization of recalcitrant pesticides. *RSC Adv.* **2017**, *7*, 45885–45895. [CrossRef]

314. Bharti; Jangwan, J.S.; Kumar, G.; Kumar, V.; Kumar, A. Abatement of organic and inorganic pollutants from drinking water by using commercial and laboratory-synthesized zinc oxide nanoparticles. *SN Appl. Sci.* **2021**, *3*, 311. [CrossRef]

315. Sharma, A.K.; Tiwari, R.K.; Gaur, M.S. Nanophotocatalytic UV degradation system for organophosphorus pesticides in water samples and analysis by Kubista model. *Arab. J. Chem.* **2016**, *9*, S1755–S1764. [CrossRef]

316. Anirudhan, T.S.; Shainy, F.; Manasa Mohan, A. Fabrication of zinc oxide nanorod incorporated carboxylic graphene/polyaniline composite and its photocatalytic activity for the effective degradation of diuron from aqueous solutions. *Sol. Energy* **2018**, *171*, 534–546. [CrossRef]

317. Khan, S.H.; Pathak, B.; Fulekar, M.H. Synthesis, characterization and photocatalytic degradation of chlorpyrifos by novel Fe: ZnO nanocomposite material. *Nanotechnol. Environ. Eng.* **2018**, *3*, 13. [CrossRef]

318. Choudhary, M.K.; Kataria, J.; Bhardwaj, V.K.; Sharma, S. Green biomimetic preparation of efficient Ag–ZnO heterojunctions with excellent photocatalytic performance under solar light irradiation: A novel biogenic-deposition-precipitation approach. *Nanoscale Adv.* **2019**, *1*, 1035–1044. [CrossRef]

319. Yari, K.; Seidmohammadi, A.; Khazaei, M.; Bhatnagar, A.; Leili, M. A comparative study for the removal of imidacloprid insecticide from water by chemical-less UVC, UVC/TiO$_2$ and UVC/ZnO processes. *J. Environ. Health Sci. Eng.* **2019**, *17*, 337–351. [CrossRef] [PubMed]

320. Dehghan, S.; Jafari, A.J.; FarzadKia, M.; Esrafili, A.; Kalantary, R.R. Visible-light-driven photocatalytic degradation of Metalaxyl by reduced graphene oxide/Fe3O4/ZnO ternary nanohybrid: Influential factors, mechanism and toxicity bioassay. *J. Photochem. Photobiol. A Chem.* **2019**, *375*, 280–292. [CrossRef]

321. Lakshmi, K.; Kadirvelu, K.; Mohan, P.S. Chemically modified electrospun nanofiber for high adsorption and effective photocatalytic decontamination of organophosphorus compounds. *J. Chem. Technol. Biotechnol.* **2019**, *94*, 3190–3200. [CrossRef]

322. Dehghan, S.; Tahergorabi, M.; Norzaee, S.; Boorboor Azimi, E.; Hasham Firooz, M.; Dadban Shahamat, Y. Preparation and photocatalytic performance of reduced graphene oxide/ZnO nanocatalyst for degradation of metalaxyl from aqueous solution: Effect of operational parameters, mineralisation and toxicity bioassay. *Int. J. Environ. Anal. Chem.* **2022**, *102*, 7112–7134. [CrossRef]

323. Aulakh, M.K.; Kaur, S.; Pal, B.; Singh, S. Morphological influence of ZnO nanostructures and their Cu loaded composites for effective photodegradation of methyl parathion. *Solid State Sci.* **2020**, *99*, 106045. [CrossRef]

324. Kumari, V.; Yadav, S.; Mittal, A.; Sharma, S.; Kumari, K.; Kumar, N. Hydrothermally synthesized nano-carrots ZnO with CeO$_2$ heterojunctions and their photocatalytic activity towards different organic pollutants. *J. Mater. Sci. Mater. Electron.* **2020**, *31*, 5227–5240. [CrossRef]

325. Serrano-Lázaro, A.; Verdín-Betancourt, F.A.; Jayaraman, V.K.; López-González, M.d.L.; Hernández-Gordillo, A.; Sierra-Santoyo, A.; Bizarro, M. Efficient photocatalytic elimination of Temephos pesticide using ZnO nanoflowers. *J. Photochem. Photobiol. A Chem.* **2020**, *393*, 112414. [CrossRef]

326. Javadimanesh, L.; Khazaei, M.; Leili, M.; Samarghandi, M.R. Using Fe/Ag nanostructures covered by Zn for the degradation of 2, 4 dichlorophenoxyacetic acid assisting with light irradiation and ozonation; optimisation and kinetic studies. *Int. J. Environ. Anal. Chem.* **2021**, 1–14. [CrossRef]

327. Saljooqi, A.; Shamspur, T.; Mostafavi, A. Synthesis and photocatalytic activity of porous ZnO stabilized by TiO$_2$ and Fe$_3$O$_4$ nanoparticles: Investigation of pesticide degradation reaction in water treatment. *Environ. Sci. Pollut. Res.* **2021**, *28*, 9146–9156. [CrossRef] [PubMed]

328. Adabavazeh, H.; Saljooqi, A.; Shamspur, T.; Mostafavi, A. Synthesis of polyaniline decorated with ZnO and CoMoO$_4$ nanoparticles for enhanced photocatalytic degradation of imidacloprid pesticide under visible light. *Polyhedron* **2021**, *198*, 115058. [CrossRef]

329. Veerakumar, P.; Sangili, A.; Saranya, K.; Pandikumar, A.; Lin, K.-C. Palladium and silver nanoparticles embedded on zinc oxide nanostars for photocatalytic degradation of pesticides and herbicides. *Chem. Eng. J.* **2021**, *410*, 128434. [CrossRef]

330. Pathania, D.; Sharma, A.; Kumar, S.; Srivastava, A.K.; Kumar, A.; Singh, L. Bio-synthesized Cu–ZnO hetro-nanostructure for catalytic degradation of organophosphate chlorpyrifos under solar illumination. *Chemosphere* **2021**, *277*, 130315. [CrossRef]

331. Yadav, S.; Jindal, J.; Mittal, A.; Sharma, S.; Kumari, K.; Kumar, N. Facile solution combustion synthesized, Li doped ZnO nanostructures for removal of abiotic contaminants. *J. Phys. Chem. Solids* **2021**, *157*, 110217. [CrossRef]

332. Ahmadifard, T.; Heydari, R.; Tarrahi, M.J.; Khorramabadi, G.S. Photocatalytic degradation of diazinon in aqueous solutions using immobilized MgO nanoparticles on concrete. *Int. J. Chem. React. Eng.* **2019**, *17*, 20180154. [CrossRef]

333. Mansourian, R.; Mousavi, S.M.; Alizadeh, S.; Sabbaghi, S. CeO$_2$/TiO$_2$/SiO$_2$ nanocatalyst for the photocatalytic and sonophotocatalytic degradation of chlorpyrifos. *Can. J. Chem. Eng.* **2022**, *100*, 451–464. [CrossRef]

334. Farrukh, M.A.; Butt, K.M.; Altaf, A. Influence of pH and temperature on structural, optical and catalytical investigations of CeO$_2$-SiO$_2$ nanoparticles. *Silicon* **2019**, *11*, 2591–2598. [CrossRef]

335. Farrukh, M.A.; Butt, K.M.; Chong, K.-K.; Chang, W.S. Photoluminescence emission behavior on the reduced band gap of Fe doping in CeO$_2$-SiO$_2$ nanocomposite and photophysical properties. *J. Saudi Chem. Soc.* **2019**, *23*, 561–575. [CrossRef]

336. Fouad, D.M.; El-Said, W.A.; Mohamed, M.B. Spectroscopic characterization of magnetic Fe$_3$O$_4$@Au core shell nanoparticles. *Spectrochim. Acta Part A Mol. Biomol. Spectrosc.* **2015**, *140*, 392–397. [CrossRef] [PubMed]

337. Adabavazeh, H.; Saljooqi, A.; Shamspur, T.; Mostafavi, A. Synthesis of KIT-5 decorated by Bi$_2$S$_3$-Fe$_3$O$_4$ photocatalyst for degradation of parathion pesticide in aqueous media: Offering a degradation model and optimization using response surface methodology (RSM). *Appl. Organomet. Chem.* **2020**, *34*, e5345. [CrossRef]

338. Merci, S.; Saljooqi, A.; Shamspur, T.; Mostafavi, A. Investigation of photocatalytic chlorpyrifos degradation by a new silica mesoporous material immobilized by WS2 and Fe3O4 nanoparticles: Application of response surface methodology. *Appl. Organomet. Chem.* **2020**, *34*, e5343. [CrossRef]

339. Soltani-Nezhad, F.; Saljooqi, A.; Mostafavi, A.; Shamspur, T. Synthesis of Fe$_3$O$_4$/CdS–ZnS nanostructure and its application for photocatalytic degradation of chlorpyrifos pesticide and brilliant green dye from aqueous solutions. *Ecotoxicol. Environ. Saf.* **2020**, *189*, 109886. [CrossRef] [PubMed]

340. Lima, M.S.; Cruz-Filho, J.F.; Noleto, L.F.; Silva, L.J.; Costa, T.M.; Luz, G.E., Jr. Synthesis, characterization and catalytic activity of Fe3O4@ WO3/SBA-15 on photodegradation of the acid dichlorophenoxyacetic (2, 4-D) under UV irradiation. *J. Environ. Chem. Eng.* **2020**, *8*, 104145. [CrossRef]

341. Saljooqi, A.; Shamspur, T.; Mostafavi, A. Synthesis of titanium nanoplate decorated by Pd and Fe$_3$O$_4$ nanoparticles immobilized on graphene oxide as a novel photocatalyst for degradation of parathion pesticide. *Polyhedron* **2020**, *179*, 114371. [CrossRef]

342. Cao, L.; Ma, D.; Zhou, Z.; Xu, C.; Cao, C.; Zhao, P.; Huang, Q. Efficient photocatalytic degradation of herbicide glyphosate in water by magnetically separable and recyclable BiOBr/Fe$_3$O$_4$ nanocomposites under visible light irradiation. *Chem. Eng. J.* **2019**, *368*, 212–222. [CrossRef]

343. Shi, E.; Xu, Z.; Wang, W.; Xu, Y.; Zhang, Y.; Yang, X.; Liu, Q.; Zeng, T.; Song, S.; Jiang, Y.; et al. Ag$_2$S-doped core-shell nanostructures of Fe$_3$O$_4$@Ag$_3$PO$_4$ ultrathin film: Major role of hole in rapid degradation of pollutants under visible light irradiation. *Chem. Eng. J.* **2019**, *366*, 123–132. [CrossRef]

344. Nekooie, R.; Ghasemi, J.B.; Badiei, A.; Shamspur, T.; Mostafavi, A.; Moradian, S. Design and synthesis of g-C$_3$N$_4$/(Cu/TiO$_2$) nanocomposite for the visible light photocatalytic degradation of endosulfan in aqueous solutions. *J. Mol. Struct.* **2022**, *1258*, 132650. [CrossRef]

345. Ebrahimpour, M.; Hassaninejad-Darzi, S.K.; Mousavi, H.Z.; Samadi-Maybodi, A. Simultaneous monitoring of the photocatalytic degradation process of trifluralin and pendimethalin herbicides by SBA-15/TiO$_2$ nanocomposite. *Environ. Nanotechnol. Monit. Manag.* **2022**, *18*, 100678. [CrossRef]

346. de la Flor, M.P.; Camarillo, R.; Martínez, F.; Jiménez, C.; Quiles, R.; Rincón, J. Synthesis and characterization of TiO$_2$/CNT/Pd: An effective sunlight photocatalyst for neonicotinoids degradation. *J. Environ. Chem. Eng.* **2021**, *9*, 106278. [CrossRef]

347. Massoud, A.; Derbalah, A.; El-Mehasseb, I.; Allah, M.S.; Ahmed, M.S.; Albrakati, A.; Elmahallawy, E.K. Photocatalytic Detoxification of Some Insecticides in Aqueous Media Using TiO2 Nanocatalyst. *Int. J. Environ. Res. Public Health* **2021**, *18*, 9278. [CrossRef]

348. Valadez-Renteria, E.; Barrera-Rendon, E.; Oliva, J.; Rodriguez-Gonzalez, V. Flexible CuS/TiO$_2$ based composites made with recycled bags and polystyrene for the efficient removal of the 4-CP pesticide from drinking water. *Sep. Purif. Technol.* **2021**, *270*, 118821. [CrossRef]

349. Ben Saber, N.; Mezni, A.; Alrooqi, A.; Altalhi, T. Ternary Pt@TiO$_2$/rGO Nanocomposite to Boost Photocatalytic Activity for Environmental and Energy Use. *J. Inorg. Organomet. Polym. Mater.* **2021**, *31*, 3802–3809. [CrossRef]

350. Hasanin, M.; Abdelhameed, R.M.; Dacrory, S.; Abou-Yousef, H.; Kamel, S. Photocatalytic degradation of pesticide intermediate using green eco-friendly amino functionalized cellulose nanocomposites. *Mater. Sci. Eng. B* **2021**, *270*, 115231. [CrossRef]

351. Vanichvattanadecha, C.; Jaroenworaluck, A.; Henpraserttae, P.; Wimuktiwan, P.; Manpetch, P.; Singhapong, W. Ordered mesoporous silica (SBA-16) supporting titania (TiO$_2$) nanoparticles for photodegradation of paraquat (PQ) herbicide. *J. Porous Mater.* **2021**, *28*, 1137–1153. [CrossRef]

352. Behera, L.; Barik, B.; Mohapatra, S. Improved photodegradation and antimicrobial activity of hydrothermally synthesized 0.2Ce-TiO2/RGO under visible light. *Colloids Surf. A Physicochem. Eng. Asp.* **2021**, *620*, 126553. [CrossRef]

353. Amiri, F.; Dehghani, M.; Amiri, Z.; Yousefinejad, S.; Azhdarpoor, A. Photocatalytic degradation of 2,4-dichlorophenoxyacetic acid from aqueous solutions by Ag$_3$PO$_4$/TiO$_2$ nanoparticles under visible light: Kinetic and thermodynamic studies. *Water Sci. Technol.* **2021**, *83*, 3110–3122. [CrossRef]

354. Vigneshwaran, S.; Sirajudheen, P.; Karthikeyan, P.; Nikitha, M.; Ramkumar, K.; Meenakshi, S. Immobilization of MIL-88(Fe) anchored TiO$_2$-chitosan(2D/2D) hybrid nanocomposite for the degradation of organophosphate pesticide: Characterization, mechanism and degradation intermediates. *J. Hazard. Mater.* **2021**, *406*, 124728. [CrossRef]

355. Meriam Suhaimy, S.H.; Lai, C.W.; Tajuddin, H.A.; Samsudin, E.M.; Johan, M.R. Impact of TiO$_2$ Nanotubes' Morphology on the Photocatalytic Degradation of Simazine Pollutant. *Materials* **2018**, *11*, 2066. [CrossRef] [PubMed]

356. Joice, J.A.I.; Aishwarya, S.; Sivakumar, T. Nano Structured Ni and Ru Impregnated TiO$_2$ Photocatalysts: Synthesis, Characterization and Photocatalytic Degradation of Neonicotinoid Insecticides. *J. Nanosci. Nanotechnol.* **2019**, *19*, 2575–2589. [CrossRef] [PubMed]

357. Ahmari, H.; Heris, S.Z.; Khayyat, M.H. The effect of titanium dioxide nanoparticles and UV irradiation on photocatalytic degradation of Imidaclopride. *Environ. Technol.* **2018**, *39*, 536–547. [CrossRef] [PubMed]

358. Eydivand, S.; Nikazar, M. Degradation of 1,2-Dichloroethane in Simulated Wastewater Solution: A Comprehensive Study by Photocatalysis Using TiO$_2$ and ZnO Nanoparticles. *Chem. Eng. Commun.* **2015**, *202*, 102–111. [CrossRef]

359. Ananpattarachai, J.; Kajitvichyanukul, P. Photocatalytic degradation of p,p'-DDT under UV and visible light using interstitial N-doped TiO$_2$. *J. Environ. Sci. Health Part B* **2015**, *50*, 247–260. [CrossRef]

360. Lopes Colpani, G.; Zanetti, M.; Zeferino, R.; Silva, L.; Mello, J.; Riella, H.; Padoin, N.; Fiori, M.; Soares, C. *Lanthanides Effects on TiO$_2$ Photocatalysts*; IntechOpen: London, UK, 2018. [CrossRef]